



(11) **EP 2 449 362 B1**

(12) **EUROPEAN PATENT SPECIFICATION**

(45) Date of publication and mention of the grant of the patent:  
**28.09.2016 Bulletin 2016/39**

(51) Int Cl.:  
**G01N 21/17** (2006.01) **A61B 5/00** (2006.01)  
**A61B 5/1455** (2006.01)

(21) Application number: **09776877.4**

(86) International application number:  
**PCT/EP2009/004687**

(22) Date of filing: **29.06.2009**

(87) International publication number:  
**WO 2011/000389 (06.01.2011 Gazette 2011/01)**

(54) **THERMOACOUSTIC IMAGING WITH QUANTITATIVE EXTRACTION OF ABSORPTION MAP**

THERMOAKUSTISCHE BILDGEBUNG MIT QUANTITATIVER EXTRAKTION EINER ABSORPTIONSKARTE

IMAGERIE THERMOACOUSTIQUE AVEC EXTRACTION QUANTITATIVE D'UNE CARTE D'ABSORPTION

(84) Designated Contracting States:  
**AT BE BG CH CY CZ DE DK EE ES FI FR GB GR HR HU IE IS IT LI LT LU LV MC MK MT NL NO PL PT RO SE SI SK TR**

(56) References cited:  
**WO-A1-2009/055095 WO-A1-2010/009747**  
**US-A1- 2006 256 339**

(43) Date of publication of application:  
**09.05.2012 Bulletin 2012/19**

(73) Proprietor: **Helmholtz Zentrum München Deutsches Forschungszentrum für Gesundheit und Umwelt (GmbH)**  
**85764 Neuherberg (DE)**

- **JAN LAUFER ET AL: "Quantitative spatially resolved measurement of tissue chromophore concentrations using photoacoustic spectroscopy: application to the measurement of blood oxygenation and haemoglobin concentration." PHYSICS IN MEDICINE AND BIOLOGY, vol. 52, no. 1, 7 January 2007 (2007-01-07), pages 141-168, XP020113117 ISSN: 0031-9155**
- **COX B T ET AL: "TWO-DIMENSIONAL QUANTITATIVE PHOTOACOUSTIC IMAGE RECONSTRUCTION OF ABSORPTION DISTRIBUTIONS IN SCATTERING MEDIA BY USE OF A SIMPLE ITERATIVE METHOD", APPLIED OPTICS, OPTICAL SOCIETY OF AMERICA, WASHINGTON, DC; US, vol. 45, no. 8, 10 March 2006 (2006-03-10), pages 1866-1875, XP001241181, ISSN: 0003-6935, DOI: 10.1364/AO.45.001866**

(72) Inventors:

- **RAZANSKY, Daniel**  
**80686 München (DE)**
- **NTZIACHRISTOS, Vasilis**  
**82166 Gräfelfing (DE)**
- **ROSENTHAL, Amir**  
**34890 Haifa (IL)**

(74) Representative: **Linsmeier, Josef et al Wallinger Ricker Schlotter Tostmann Patent- und Rechtsanwälte**  
**Zweibrückenstrasse 5-7**  
**80331 München (DE)**

Note: Within nine months of the publication of the mention of the grant of the European patent in the European Patent Bulletin, any person may give notice to the European Patent Office of opposition to that patent, in accordance with the Implementing Regulations. Notice of opposition shall not be deemed to have been filed until the opposition fee has been paid. (Art. 99(1) European Patent Convention).

**EP 2 449 362 B1**

**Description**Subject of the invention

5 **[0001]** The invention relates to methods of creating thermoacoustic images of an object, wherein a quantitative image representing a local map of absorption within the object is reconstructed based on thermoacoustic signals obtained from a mechanical wave response to a delivery of electromagnetic energy into the imaged object. Furthermore, the invention relates to thermoacoustic imaging devices configured for conducting the above methods. Applications of the invention are available e. g. in medical imaging or material investigations. In particular, the invention can be used for accurate extraction of biomarker concentration in noninvasive small animal and clinical imaging, e. g. for characterization of vascular trees, tumor angiogenesis, blood oxygenation or in molecular imaging studies with various targeted contrast agents, including dyes, light-absorbing nano-particles and fluorochromes.

Technical background

15 **[0002]** Thermoacoustic imaging is a fast evolving non-invasive modality for high-resolution mapping of local energy deposition in tissue. In particular, optoacoustic (or photoacoustic) tomography aims at reconstructing maps of local optical absorption coefficient of tissue, which can subsequently be related to the concentration of certain intrinsic and exogenously-administered biomarkers and probes. The imaging is performed by illuminating the object or region of interest with short high-power electromagnetic pulses, in particular laser pulses, thus creating an instantaneous temperature elevation and thermal expansion within it. As a result, high-frequency acoustic fields are formed that propagate towards the object's boundary where they can be subsequently recorded. In this way, an image representing local energy deposition within the object can be reconstructed by collecting tomographic information around the object and using optoacoustic inversion algorithms.

20 **[0003]** While the image formation in optoacoustics can be performed in several ways, all of them require some mathematical inversion for image formation from raw measurements of the optoacoustic response. Ideally, the reconstructed image should represent a quantitative map of the underlying absorption properties of the imaged tissue, which can be subsequently related to distribution of various tissue chromophores and biomarkers. However, in most cases, the detected acoustic signals will rather represent to the overall local energy deposition in the imaged object. Thus, the initial optoacoustic image requires further analysis to extract the relevant information. One apparent difficulty is the highly heterogeneous nature of common biological tissues in the visible and near-infrared spectra. This in turn causes highly non-uniform distribution of excitation light within the imaged object owing to scattering and attenuation. In addition, inaccuracies in the currently used optoacoustic inversion models further hinder image quantification.

25 **[0004]** With further detail, current optoacoustic inversion techniques, which produce the deposited energy image from the acoustic fields, suffer from quantification inaccuracy, low spatial resolution, or inflexibility owing to the absence of appropriate methods to accurately account for experimental and physical propagation factors. Algorithms that currently exist for inversion and image formation can be divided into two groups: those which are based on a closed form analytical solution of the optoacoustic wave equation and those which are based on numerical calculations.

30 **[0005]** The first kind of algorithms refers to back-projection algorithms, in which the reconstruction of the optoacoustic image is given as an integral over the measured signals similar to linear Radon-based transformations. These reconstruction methods are usually based on several approximations to the exact optoacoustic equation, thus create substantial artifacts in the reconstruction. Moreover, the back-projections algorithms are incapable of incorporating multiple instrumentation-based factors into the inversion. For example, it may not be possible to directly take into account the frequency response of the ultrasonic detector or its finite size in the back-projection algorithms.

35 **[0006]** The second kind of algorithms is model-based inversion in which the acoustic propagation problem is solved numerically and iteratively in either the frequency or time domains by using e.g. finite-elements method. Model-based thermoacoustic inversion schemes were previously attempted by H. Jiang et al. ("J. Opt. Soc. Am." vol. A 23, 2006, p. 878-888) and by G. Paltauf et al. ("The Journal of the Acoustical Society of America", vol. 112(4), 2002, p. 1536-44). However, the computational complexity involved with these particular methods has limited their achievable resolution and hindered practical implementations.

40 **[0007]** Since in most realistic imaging scenarios it is practically impossible to uniformly illuminate the entire region of interest, the initially formed image will represent a coupled map of energy deposition in tissue and absorption, rather than the required quantified absorption coefficient values. In other words, the thermoacoustic image will comprise a product between the optical absorption and the light fluence within the object. Thus, targets deep in the object may appear weaker than targets having similar optical absorption but located close to the illuminated surface. Quantitative reconstructions, especially of volumetric phenomena, were not previously possible owing to limitations in both optoacoustic inversion algorithms, image normalization methods and corresponding system implementations. These inaccuracies limit applicable areas of conventional (qualitative) optoacoustic imaging. Consequently, systems reported so far

for optoacoustic imaging compromise the image quality and quantification, a performance that worsens with depth or volumetric imaging.

**[0008]** Moreover, when analyzing multi-spectral optoacoustic images, i.e. images obtained for several excitation wavelengths, spectral changes in the light fluence may dominate the optoacoustic images and obfuscate the absorption spectrum of targets of interests. This limits the use of Multi-Spectral Optoacoustic Tomography (MSOT), which is described e. g. in PCT/EP2008/006142 (unpublished on the priority date of the present specification), for mapping the concentration of various targets with spectrally dependant absorptions.

**[0009]** Methods have been proposed so far for the extraction of the absorption coefficient and quantification improvement. Some approaches are based on solving the diffusion equation that governs light propagation in order to find and correct for light distribution within the object (B. T. Cox et al. in "Applied Optics" vol. 45, p. 1866-1875, 2006; B. T. Cox BTet al in "Proc SPIE" 6437, 64371T-1-10, 2007). Once a hypothesized light distribution solution is found, it is used to normalize the optoacoustic image and to extract the absorption coefficient. As a further step, the extracted absorption can be used to recalculate the light distribution within the object, which in turn is used to re-normalize the optoacoustic image. This process can be repeated in an iterative manner until convergence is achieved. However, the above methods rely on empirical assumptions regarding optical properties of the tissue and other experimental parameters. Therefore they suffer from convergence instability that limits the ability for robust quantification accuracy (Jetzfellner et al. in "Appl. Phys. Lett." 95(1), 2009).

**[0010]** The main deficiency of optoacoustic image normalization methods is that they rely on a light fluence distribution that is modeled based on hypothesized light propagation equations, such as the light diffusion equation. However, these equations require accurate prior knowledge of the optical properties of the medium, which are usually largely unknown, in particular scattering but also absorption. In most cases, an estimated value or structure is prescribed to the optical parameters of the medium. In practice, it has been found however that even small errors in the assigned optical properties can lead to large errors in the reconstruction. Moreover, if an iterative self-correcting approach is applied, convergence to accurate values is rarely possible owing to modeling inaccuracies. Thus, as to date, reliable performance has not yet been demonstrated using these techniques for in-vivo data, i.e. for media where light distribution is spatially heterogeneous.

**[0011]** The above limitations are not restricted to optoacoustics. The corresponding disadvantages generally occur in other thermoacoustic imaging methods wherein e. g. radiofrequency pulses are used for delivering energy to the object instead of the object illumination with laser pulses.

#### Objective of the invention

**[0012]** The objective of the invention is to provide improved methods and preferred geometry embodiments for thermoacoustic imaging capable of avoiding disadvantages and restrictions of conventional qualitative reconstruction techniques. In particular, it is the objective of the invention to provide accurate thermoacoustic imaging methods being capable of quantitative imaging with increased precision and reproducibility, not only in surface and subsurface regions, but also volumetrically in entire objects. Furthermore, the objective of the invention is to provide thermoacoustic imaging device implementations, which are capable of avoiding disadvantages and restrictions of conventional techniques.

#### Summary of the invention

**[0013]** The above objectives are achieved with thermoacoustic imaging methods and/or thermoacoustic imaging devices comprising the features of the independent claims, respectively. Preferred embodiments of the invention are defined in the dependent claims.

**[0014]** According to a first aspect of the invention, a method of thermoacoustic imaging of an object is described, wherein an energy deposition image is subjected to a decomposition into a quantitative absorption image representing a geometric distribution of a local absorption coefficient in the object and at least one further image component. Firstly, thermoacoustic signals are provided representing a mechanical wave response to a delivery of electromagnetic energy (excitation energy) into the imaged object. Provision of the thermoacoustic signals comprises e. g. collecting or recording the signals with an imaging device or delivering the signals from a data source. Subsequently, based on the thermoacoustic signals at least one energy deposition image representing a local energy absorption within the object is reconstructed. The reconstruction comprises a matrix-based optoacoustic inversion according to the second aspect of the invention outlined below. Finally, the energy deposition image is subjected to the decomposition into the quantitative absorption image and the at least one further image component.

**[0015]** Depending on the wavelength of the excitation energy used, the local absorption coefficient distribution (absorption image) comprises e. g. an optical absorption distribution or an electric conductivity distribution. The at least one further image component typically comprises a distribution of the excitation energy in the object. Alternatively or additionally, the at least one further image component comprises an image of one or more from the following - a distribution

of the optical scattering coefficient, a distribution of speed of sound, an image representing local polarization state, an electric or magnetic field distribution, a dielectric constant distribution, a thermoelastic expansion coefficient distribution, a heat capacity distribution, and a distribution of a certain biomarker.

5 [0016] The image decomposition representing the essential part of the first aspect of the invention provides a new quantification methodology of thermoacoustic tomographic reconstructions under highly heterogeneous illumination conditions, as occurring e. g. with realistic wholebody imaging scenarios. Advantageously, the inventive image decomposition method does not depend on selecting an accurate photon-propagation model to account for the fluence non-uniformities within the medium. Instead, it decomposes the image to its principal components by using techniques from the field of sparse representation. The inventive decomposition method relies on different spatial characteristics of the absorption coefficient and the energy density (fluence), in particular optical energy or photon density, within the medium. 10 The inventors have found that the fluence is smooth and global, while the absorption coefficient has more localized and often sharp spatial transients in most imaging applications like medical imaging or imaging in material sciences. By using the sparse-representation based decomposition, these different characteristics are exploited to extract both the absorption coefficient and the energy deposition density within the imaged object from the thermoacoustic image. In contrast to previous methods, this image normalization method is not based on the solution of theoretical light transport equations and offers robust performance, as it does not require explicit knowledge of the illumination geometry, optical properties of the object and other unknown or loosely defined experimental parameters. The inventive method is therefore ideally suited for practical implementations in varying complexity tomographic schemes including multi-projection illumination systems and multi-spectral optoacoustic tomography studies of tissue biomarkers.

20 [0017] According to a second aspect of the invention, a method of thermoacoustic imaging of an object is provided, wherein thermoacoustic signals representing a mechanical wave response to a delivery of electromagnetic energy to the object are used for reconstructing an energy deposition image representing a local energy deposition within the object and wherein the reconstructing step includes a matrix-based optoacoustic inversion of the thermoacoustic signals utilizing a forward model matrix.

25 [0018] The matrix-based optoacoustic inversion representing the essential part of the second aspect of the invention provides a novel semi-analytical model-based inversion method for quantitative thermoacoustic image reconstruction. In contrast to backprojection-like algorithms, the inventive method is not based on an analytical solution to the inverse problem. Instead, the forward problem is reformulated in matrix relation, which is subsequently inverted. Advantageously, thermoacoustic signal generation and propagation presents a linear forward problem, therefore this type of optimization problem has only one single minimum. In addition, the model matrix is sparse, thus enabling efficient inversion algorithms to be used. Ideally, the inversion can yield artifact-free quantified thermoacoustic image reconstructions. As a further advantage, many additional linear effects can be added to the model matrix, while using the same matrix-inversion algorithm. Thus, the forward model is highly flexible and can be used to model a variety of linear attenuation and dispersion effects, for example by taking the frequency response and spatial response of the detector into account as well as 35 acoustic coupling, dispersion and other propagation aspects.

[0019] The semi-analytical solution presented with the invention is exact for piecewise planar acoustic-source functions. Thus, the solution is exact for a planar interpolation of the acoustic-source functions. This significantly improves the accuracy and computational speed associated with the forward model. Using this solution, the model matrix can be constructed, connecting the measured acoustic signals with the thermoacoustic image. By inverting the matrix relation, 40 the thermoacoustic image is recovered. The matrix elements depend only on the setup geometry, and thus can be calculated before the experiment is performed. The inversion of the matrix relation can also be preformed beforehand by calculating the pseudo-inverse of the matrix. Once the experiment is performed, the inversion amounts to multiplying the pre-calculated pseudo-inverse with a vector containing the measured data - a computation that can in principle be performed in real time. Numerical and experimental tests have shown that the inventive reconstruction algorithm does not suffer from backprojection-related reconstruction artifacts and renders an accurate high-resolution map of laser energy deposition in the imaged object.

[0020] Apparently, the matrix model-based approach has several advantages over back-projection algorithms. First, it eliminates image artifacts associated with the approximated backprojection formulations, i.e. no negative absorption values are produced and the reconstructed image corresponds to the true light attenuation and energy deposition within 50 the object. Clearly, since back-projection falsely emphasizes edges and fast image variations by producing large negative overshoots, it is capable of producing 'good looking' high-contrast images. However, due to its approximate formulation, it fails to reproduce the correct and quantitative image of the actual laser energy deposition in tissue and the underlining optical absorption values. This property is especially important for quantitative imaging applications, i.e. molecular imaging studies, in which obtaining the correct absorption maps is of high importance. Secondly, the inventive method admits generalization of the forward solution to a more comprehensive acoustic propagation models without changing the inversion procedure. Finally and importantly, the model-based inversion can be seamlessly adapted to any detection geometry. Unlike in the conventional analytical inversion formulation, the position of the detectors is not restricted to specific geometries.

5 [0021] According to a third aspect of the invention, an imaging device for thermoacoustic imaging of an object comprises a signal collecting device, a reconstruction device, and a decomposition device. The imaging device in particular is configured for implementing one of the methods of the above first and second aspects. The signal collecting device is an apparatus which is configured for collecting thermoacoustic signals in response to a delivery of electromagnetic energy into the imaged object. The signal collecting device is connected with the reconstruction device, which is arranged for processing the thermoacoustic signals. The reconstruction device is adapted for reconstructing an energy deposition image representing a local energy deposition within the object based on collected thermoacoustic signals. For implementing the above second aspect of the invention, the reconstruction device comprises an inversion circuit being adapted for subjecting the thermoacoustic signals to a matrix-based optoacoustic inversion utilizing an inverted model matrix. 10 Furthermore, the reconstruction device is connected with the decomposition device, which is adapted for decomposing the energy deposition image into a quantitative absorption image representing a distribution of a local absorption coefficient in the object and at least one further image component.

15 [0022] According to a fourth aspect of the invention, an imaging device for thermoacoustic imaging of an object comprises a reconstruction device being adapted for reconstructing the energy deposition image representing a local energy deposition within the object based on thermoacoustic signals, wherein the reconstruction device comprises an inversion circuit being adapted for subjecting the thermoacoustic signals to a matrix-based optoacoustic inversion utilizing an inverted model matrix.

20 [0023] With the above inventive aspects, the current invention identifies systems and methods that achieve mapping of the absorbed energy deposition within the object from the measured acoustic signals and extract the absorption coefficient from this mapping by sparsely representing the mapping in a function library (function basis). Each of the aspects represents an independent subject of the invention. However, their combination is preferably implemented for achieving maximum imaging performance.

25 [0024] Preferably, the delivered electromagnetic energy comprises photon energy in the optical spectrum, i.e. the object is illuminated with light. The illumination light comprises at least one characteristic wavelength of at least 1 nm, preferably at least 400 nm, particularly preferred at least 650 nm, and below 5000 nm, preferably below 1200 nm, particularly preferred below 850 nm. For this embodiment, the signal collecting device includes a laser source device being adapted for emitting light pulses, preferably in the visible or near-infrared spectra. The light pulses preferably have a duration below 1  $\mu$ s, particularly preferred below 50 ns.

30 [0025] Typically, the illumination light comprises one single illumination wavelength and/or one single light polarization. Accordingly, the energy deposition image can be reconstructed based on the thermoacoustic signals acquired at the single illumination wavelength and/or the single light polarization.

35 [0026] Alternatively, the information content of the inventive quantitative imaging advantageously can be increased if the illumination light comprises multiple different excitation wavelengths and/or multiple different light polarizations. With this embodiment, multiple energy deposition images can be separately reconstructed based on the thermoacoustic signals separately acquired at the different illumination wavelengths and/or the different light/field polarizations. As a further option, the energy deposition image can be reconstructed based on a combination of the thermoacoustic signals acquired at the different illumination wavelengths and/or the different light/field polarizations. The combination of the thermoacoustic signals comprises linear or nonlinear signal superpositions, e.g. subtractions, summations, products, ratios or the like.

40 [0027] Alternatively, the delivered electromagnetic energy may comprise pulses in the radiofrequency or microwave spectral regions, preferably with pulse durations below 1  $\mu$ s, most preferably with pulse durations below 50 ns. Accordingly, the signal collecting device may include radiation source being adapted for irradiating the imaged object with the radiofrequency pulses.

45 [0028] According to a further embodiment of the invention, the thermoacoustic signals can be subjected to a pre-processing before the image reconstruction. Advantageously, pre-processing by an analog or digital signal processing operation, e.g. filtering, integration, differentiation, may improve the result of the image reconstruction.

50 [0029] With the inventive image reconstructing step using the matrix-based optoacoustic inversion of the thermoacoustic signals, the elements of the model matrix can be chosen in dependency on linear effects influencing the thermoacoustic signal generation and propagation. According to a preferred variant of the invention, the model matrix is constructed in dependency on the geometry of a mechanical wave detector device collecting the thermoacoustic signals. Alternatively or additionally, the model matrix is constructed in dependency on at least one of an acoustic heterogeneity of the object, a geometric profile of the delivered electromagnetic energy in the imaged object, a frequency response of an acoustic-signal recording device utilized for collecting the thermoacoustic signals and a result of the decomposing step. Advantageously, the model matrix elements are mostly independent of the absorption properties of the object.

55 [0030] According to a particularly preferred embodiment of the invention, a logarithmic representation of the reconstructed energy deposition image is provided for the image decomposing step. Thus, the contributions of the absorption image and the at least one further image component are obtained as separate summands. Subsequently, the energy deposition image decomposing step comprises a calculation of the quantitative absorption image and the at least one

further image component as summands of the logarithmic representation of the energy deposition image. For conducting these steps, the inventive imaging device includes the decomposition device including a logarithm circuit and a processor calculating the quantitative absorption image and the at least one further image component.

5 **[0031]** Each of the summands preferably is provided as expansions in complementary libraries. The quantitative absorption image is represented as an expansion in a first library (a collection of functions, e.g. a function basis), while the at least one further image component is represented as an expansion in at least one further library. The libraries are complementary libraries if the representation of the quantitative absorption image in the at least one further library requires a significantly higher number of library functions than what is required when using the first library (and vice versa, i.e. the representation of the at least one further image component in the first library requires a significantly higher number of library functions than what is required when using the at least one further library). Advantageously, the expansion coefficients of the representation in the complementary libraries can be obtained with a minimization algorithm.

10 **[0032]** As a particular advantage of the invention, various types of image components can be separated from the absorption image as a result of the decomposing step. Preferably, the at the least one further image component comprises an excitation light fluence distribution image and/or a distribution of the optical scattering coefficient in the object. In this case, artefacts due to scattering of the energy deposition in the objects can be avoided. Alternatively, the at the least one further image component comprises an image representing a local polarization state (e.g. a birefringence or dichroism state of the object), an electric or magnetic field distribution, a speed of sound distribution, a dielectric constant distribution, a thermoelastic expansion coefficient distribution, and/or a heat capacity distribution in the object.

15 **[0033]** Particular benefits for medical imaging are achieved if the at least one further image component comprises an image representing a local state of the object, in particular a physiological state of biological tissue. The physiological state may represent e. g. a disease progression, an oxygenation state and/or a metabolic state. As a further alternative, the at least one further image component may comprise an image representing a spatial distribution of a tissue biomarker, e. g. an extrinsically administered molecular agent, a fluorescent protein, a functionalized particle, and/or a chromogenic assay in the object.

20 **[0034]** The provision of the thermoacoustic signals comprises a signal collection (measuring step). The object to be imaged is irradiated by electromagnetic energy, e. g. by laser pulses, and the thermoacoustic signals produced in response to the irradiation are recorded. Advantageously, the signal collection can be performed as it is known as such from conventional thermoacoustic imaging, in particular optoacoustic imaging. To this end, the signal collecting device comprises an electromagnetic energy source and an acoustic signal recording device with a detector array and/or a single detector, including at least one acoustic detection element. Preferably, an acoustically-matched membrane is provided separating the imaged object from a liquid medium, like e. g. water or a physiological solution, where the at least one acoustic detection element is located. Advantageously, the membrane allows for the object to be imaged without being immersed into the liquid medium.

25 **[0035]** Advantageously, the inventive imaging device can be provided with hardware circuits being configured to conduct the methods of above first or second aspects of the invention. As an example, the inversion circuit for matrix-based optoacoustic inversion of the thermoacoustic signals may include at least one of a matrix storage module storing the model matrix and/or its inverse or a truncated version of each (or both) of these matrices, containing the most energetic elements of these matrices, and an adjustment device being adapted for adjusting the model matrix in dependency on imaging conditions, e. g. on at least one of an acoustic heterogeneity of the object, a geometric profile of the illumination of the imaged object by the light pulses, a frequency and/or spatial response of a acoustic signal recording device utilized for collecting the thermoacoustic signals and an output of the decomposition device. Furthermore, the reconstruction device may comprise an iteration circuit being adapted for implementing an iterative propagation model-based simulation.

30 **[0036]** According to a further preferred embodiment of the inventive imaging device, the acoustic signal recording device and the object are movable relative to each other. The steps of collecting the thermoacoustic signals, reconstructing the energy deposition image and decomposing the image can be repeated with varying geometric orientation and/or position of the signal recording device and the object relative to each other.

35 **[0037]** The inventive decomposition step can be used as a first analysis step also in the Multi-Spectral Optoacoustic Tomography (MSOT) method. With regard to details of implementing the MSOT method, PCT/EP2008/006142 is mentioned.

40 **[0038]** In one of the preferred embodiments, the decomposition is performed on e.g. a difference between images obtained for different excitation wavelengths normalized by their sum. This eliminates possible negative effects of the spectral dependence of light fluence during spectral decomposition.

45 **[0039]** In order to effectively implement the proposed methods, appropriate geometries to optimally illuminate and collect data from tissues are required to ensure that sufficient amount of information is present. For example, the temporal and spatial resolutions with which the acoustic signals are measured preferably correspond to the desired pixel/voxel resolution in the reconstructed image. In addition, any parts of the object that are to be imaged preferably are illuminated as uniformly as possible for as many acoustic measurements as possible. This is preferred since the advantages of the

method become apparent when achieving high quality whole-body (volumetric or cross-sectional) images but may not be essential for surface-limited imaging with relatively uniform excitation energy deposition, as is more commonly enabled currently. Therefore, system that can optimally implement the method is proposed as well, to illustrate the key components required for accurate implementation.

5 **[0040]** In contrast to the previous art, the inventive method enables *quantitative*, rather than *qualitative*, mapping of the absorption coefficient e. g. in biological tissue. As such, it is essential for *in-vivo* whole-body imaging applications, especially those dealing with deep tissue small animal imaging and clinical imaging. For the latter case, it is essential to provide also technology that effectively addresses aspects associated with volumetric imaging, i.e. imaging of large (compared to the light transport mean free path length (MFPL)) samples, when the actual optical properties of the imaged object and other experimental parameters are poorly determined or unknown or even varying during the course of the experiment.

10 **[0041]** Further subjects of the invention are a computer program residing on a computer-readable medium, with a program code for carrying out the method according to the above first or second aspects of the invention, and an apparatus comprising a computer-readable storage medium containing program instructions for carrying out the inventive methods.

Brief description of the drawings

20 **[0042]** Further details and advantages of the invention are described in the following with reference to the attached drawings, which show in:

Figure 1: an overview of main steps of imaging methods according to embodiments of the invention,

25 Figures 2 and 3: schematic illustration of embodiments of the inventive imaging device;

Figure 4: a schematic illustration of main components of a signal processor device included in the inventive imaging device;

30 Figure 5: a graphical illustration of a grid used for tiling an x-y reconstruction plane;

Figures 6 and 7: graphical illustrations of different components in optoacoustic images and their sparse representation in complementary libraries;

35 Figures 8 and 9: schematic illustrations of alternative variants of an energy deposition reconstruction device included in the inventive imaging device; and

Figure 10: a schematic illustration of main components of an absorption image decomposition device included in the inventive imaging device.

40 Preferred embodiments of the invention

**[0043]** Preferred embodiments of the invention are described in the following with exemplary reference to optoacoustic tomography. The invention is not restricted to these embodiments, but can be equally applied to other methods utilizing opto- or thermoacoustic interactions, for instance Photo-Acoustic Tomography (PAT), multispectral optoacoustic tomography (MSOT), thermoacoustic tomography (TAT) or Near-Field Radiofrequency Tomography (NRT).

1. Overview

50 **[0044]** The mapping of the absorption coefficient of an object, e. g. a human or animal body or a part thereof using optoacoustic imaging can be described in three general steps. A schematic description of the steps is given in Figure 1. The first step S1 comprises data acquisition and entails illuminating the imaged object using high-power short-pulse lasers and measuring the formed acoustic waves by detector located in proximity of the object's boundary. The further two steps S2 and S3 are the core of the invention described herein and involve processing the measured data to obtain a two- or three-dimensional map of the optical absorption coefficient within the object. Conducting the second and third steps S2 and S3 immediately after the first signal collection step is an optional feature of the invention. Alternatively, the inventive image reconstruction can be applied to data obtained from an image data storage and/or via a computer network.

55 **[0045]** In the second step S2, the model-based acoustic-inversion method is used to backtrack the acoustic wave propagation and find the optoacoustic sources that were created within the object as a result of pulsed light absorption.

Because the relation between the measured acoustic field and the optoacoustic sources is linear, it is discretized into a matrix form in order to facilitate numerical calculations. The matrix may include all the linear effects involving the acoustic propagation and detection. For example, the frequency response of the acoustic detector, speed of sound heterogeneities, or acoustic attenuation and dispersion can be accounted for in the matrix relation. Once the matrix is calculated, various inversion schemes may be used for inverting the matrix relation and obtaining the distribution (image) of the optoacoustic sources within the object.

**[0046]** The optoacoustic sources' amplitudes are proportional to the amount of energy absorbed within the object. Thus, mapping the optoacoustic sources does not directly yield the absorption coefficient, but rather the product between the absorption coefficient and light fluence. As a result, the optoacoustic source image is biased toward the regions of the objects that are better lit. The third step S3 comprises eliminating this bias, thus obtaining an image of the absorption coefficient from the optoacoustic source image. This step S3 is based on the inventive decomposition method that exploits the different spatial properties of the absorption coefficient and light fluence within the body which dictate different sparse representations for these two functions. Because of light diffusion, the fluence may be regarded as a slowly varying function, whereas the absorption coefficient may have sharp transients. In multi-spectral measurements, the third step may be also applied to the normalized difference of optoacoustic images obtained for different excitation wavelengths.

**[0047]** In the preferred embodiment, the method decomposes the optoacoustic image by calculating the sparsest representation of its logarithm over the unification of the two libraries. The sparsest representation can be found by using one of several available algorithms. In this representation, all the elements that are included in the library of the absorption coefficient can be used to effectively extract the quantified absorption coefficient image.

**[0048]** Figure 2 schematically illustrates an embodiment of an imaging device 100 for thermoacoustic imaging of an object 1. The imaging device 100 comprises a signal collecting device 10, an image processor device 20 and optionally a further control device 30. The components 20, 30 can be implemented within a common hardware unit. The signal collecting device 10 comprises an electromagnetic energy source, like at least one laser source 11, emitting pulses with a duration lower than 50 ns and an acoustic signal recording device 12 (detector device) with at least one acoustic detection element. The laser source 11 can be tuned to different wavelengths so that multispectral information can be collected from the object 1, e. g. for localization of distinct spectral signatures of tissue biomarkers.

**[0049]** Details of the signal collecting device 10 can be implemented as described by D. Razansky and V. Ntziachristos in "Med. Phys." Vol. 34, 2007, pp. 4293-4301. In particular, the laser source 11 may comprise a tunable optical parametric oscillator (OPO) laser providing < 10 ns duration pulses with repetition frequencies in the range 10 - 100 Hz in the visible (400-700 nm) or near-infrared (700-1400 nm) spectra. As an example, the illumination wavelength was set to 750 nm while the output energy was kept below 25 mJ per pulse while the output near-infrared beam was expanded so its average diameter in the sample plane was about 2 cm.

**[0050]** In order to illuminate the region of interest in object 1 as uniformly as possible, the laser beam can be expanded to cover the entire object's diameter and split into two or more beams, illuminating the object 1 from different directions. Furthermore, delivery of light into the object 1 can be done by e.g. optical fiber or fiber bundle having multiple arms or by means of transmitting free beams via optical arrangement of mirrors, beam splitters, diffusers etc.

**[0051]** The acoustic signal recording device 12 is arranged in acoustic contact with a surface of the object, e. g. using a sound transmitting substance, like a gel, or a liquid. The object 1 can be partially or completely separated from the liquid as shown in Figure 3. The acoustic signal recording device 12 comprises e.g. a single piezoelectric-type point detector. For collection of the signals over 360° projections, the object 1 can be rotated on a stage with certain angular increments (e.g. 2 or 3 degrees), while the detector is placed at a distance of e.g. 40 mm from the center of rotation. The acoustic signal recording device 12 can be translated along a vertical axis over a predetermined number of points to acquire data for three-dimensional reconstruction in cylindrical scanning configuration (see above publication of D. Razansky and V. Ntziachristos). The detector's surface can alternatively resemble different focusing shapes (e.g. cylindrical, spherical) so that the optoacoustic signals can be preferentially collected from different areas of interest (line, plane etc). Due to ultrawideband nature of typical optoacoustic signals, the detector should ideally have a broad effective (-6db) bandwidth, e.g. between 1 - 10 MHz, more preferably between 200 kHz - 30MHz, most preferably between 50 kHz - 100 MHz. Alternatively, the acoustic signal recording device 12 comprises a detector array with a plurality of acoustic detection elements in order to simultaneously collect information from multiple projection angles. The detection of optoacoustic responses can alternatively be made by optical means, e.g. by using interferometric devices sensitive to pressure variations, e.g. Fabry-Perot films and other multi-layered structures.

**[0052]** As an example, the full-width-at-half-maximum (FWHM) of the detector's frequency response can be at 3.5 MHz, which corresponds to a diffraction-limited spatial resolution of about 200 μm. Frequency response of the detector does not only limit the spatial resolution of the reconstructed images, but can also distort the shape of the detected signals and thus introduce additional image artifacts. Therefore, the frequency response is taken into account during the reconstruction process (see below).

**[0053]** The time-resolved thermoacoustic signals (typically electrical voltage signals), recorded by the acoustic signal

recording device 12 can be digitized, averaged (for noise suppression) and transmitted to the central processing unit (CPU) of the image processor device 20 responsible for quantitative image reconstruction.

**[0054]** According to Figure 3, the object 1 illuminated with the laser source 11 is placed on top of a transparent membrane 13. The membrane 13 is made of optically transparent material that also does not significantly alter propagation of sound, e.g. acoustically-matched membrane made of polyvinyl chloride plastisol (PVCP) or thin films of polyethylene. In this way, an efficient transmission of both laser radiation and the induced optoacoustic response is facilitated. The membrane 13 also ensures that the imaged object 1 can be conveniently placed for imaging without direct contact with water. The membrane 13 is placed in contact with a water tank 14, into which the detector array 12 is immersed. The detector array 12 is a curved array with 64 acoustic detection elements 15, which form for example 180° arc that surrounds the object 1. In example of Figure 3, all the acoustic detection elements 15 are cylindrically focused in the detection plane to allow for simultaneous collection of signals from a two-dimensional detection plane (drawing plane). The device will therefore collect two-dimensional data in real time.

**[0055]** The main components of the image processor device 20 are illustrated in Figure 4. After pre-processing collected raw signals in the signal interface unit 21, the thermoacoustic signals are delivered to the reconstruction device 22 quantitatively reconstructing the energy deposition image (see below 2.). Subsequently, the energy deposition image is processed in the decomposition device 23 decomposing the energy deposition image into a quantitative absorption image and at least one further image component (see below 3., 4.). Finally, the quantitative absorption image data are output via the interface 24, followed e. g. by further data handling, like e. g. a data storage, image data recording, image display or image output, like printing.

## 2. Semi-analytical model-based optoacoustic inversion method for quantitative thermoacoustic tomography

**[0056]** The forward problem of optoacoustic tomography amounts to modeling the acoustic fields created by the instantaneous heating and relaxation effect of the laser irradiation. Under the condition of thermal confinement, the temperature increase in each part of the irradiated object is not affected by temperature increase in neighboring regions, i.e. heat conductance is negligible. This condition is usually fulfilled for laser pulses with duration lower than 1 μs and guarantees that the acoustic sources created in the object are proportional to the absorbed optical energy. Under this condition, and neglecting acoustic losses, the propagation equation for the acoustic fields is given by

$$\frac{\partial^2 p(r,t)}{\partial t^2} - c^2 \rho \nabla \cdot \left( \frac{1}{\rho} \nabla p(r,t) \right) = \Gamma \frac{\partial H(r,t)}{\partial t}, \quad (1)$$

where  $c$  and  $\rho$  are velocity of sound in tissue and its density,  $\Gamma$  is the Grüneisen parameter, and  $h$  is the amount of energy absorbed in the tissue per unit volume and per unit time.  $H$  can be represented as a product between its spatial and temporal components  $h, h_t$ . In the present analysis, propagation of acoustic fields in acoustically homogenous medium can be assumed. Under this assumption, the above equation takes the form of

$$\frac{\partial^2 p(r,t)}{\partial t^2} - c^2 \nabla^2 p(r,t) = \Gamma h(r) \frac{\partial h_t(t)}{\partial t}. \quad (2)$$

**[0057]** In most practical cases, the duration of the optical pulse is short enough to be approximated by a delta function, namely  $h_t(t) = \delta(t)$ . In this case, i. e. assuming the heating due to the laser pulse is instantaneous, and that the medium is acoustically homogeneous, an analytical solution is given by a Poisson-type integral, wherein the acoustic pressure measured at a coordinate  $x$  and at a time  $t$  fulfills the following equation:

$$p(x,t) \propto \frac{\partial}{\partial t} \int_{R=vt} \frac{h(x')}{R} dA', \quad (3)$$

where  $R = |x-x'|$ ,  $v$  is the velocity of sound in the medium, and  $h(x)$  is the optoacoustic image. When the measurement is performed in 3D, the integration in Eq. (3) is performed over a sphere. When the measurement is performed in 2D, the integration in Eq. (3) is performed over a circle. In the following description, the 2D case is illustrated, although the same concepts can be generalized for the 3D case. In particular, the solutions can be readily generalized to 3D by collecting optoacoustic signals that originate at different planes.

**[0058]** In a two-dimensional (2D) geometry, for which all the sources lie in a plane, the integration is performed over

a circle. For a given sensor position  $r=(x_0,y_0)$ , the integral in Eq. (3) can be explicitly rewritten as

$$\int_{R=ct} \frac{h(r')}{R} dA' = \int_{\theta_1}^{\theta_2} h(x_0 + R \cos \theta, y_0 + R \sin \theta) d\theta \quad (4)$$

**[0059]** In both 2D and 3D geometries, the calculation of Eq. (4) poses numerical difficulties that stem from the inconsistency of the grid with the surface on which the integral is to be calculated. Calculating the derivative of the integral only exacerbates the numerical problems. Typically, in order to accurately calculate Eq.(4), the resolution of the grid should be considerably higher than what otherwise be required to accurately represent  $h(r)$ . This readily results in computational inefficiency of the solution to the forward problem.

**[0060]** According to the invention, a grid is defined to discretely represent  $h(x)$ , and the grid coordinates are marked by  $x_i$ . In order to calculate the integral in Eq. (3), a close form approximation  $h(x)$  is used for coordinates which are not on the grid. The only requirement for that approximation is that for any given coordinate  $x'$ , the value of  $h(x')$  be a linear superposition of the values of  $h(x)$  at the mesh coordinates:

$$h(x') = \sum_{i=n}^m f_i(x_n, \dots, x_m, x') h(x_i) \quad (5)$$

**[0061]** Since the mesh points are predetermined, the value of the function  $f_i(x_n, \dots, x_m)$  is independent of the measured data. Substituting Eq. (5) into Eq. (3), a linear connection between the measured acoustic pressure and the optoacoustic image is obtained:

$$p(x, t) \propto \sum_{i=k}^l g_i(x, t, x_k, \dots, x_l) h(x_i), \quad (6)$$

where the values of  $g_i(x, t, x_k, \dots, x_l)$  are calculated by solving the integral in Eq. (3) with the functions  $f_i(x_n, \dots, x_m, x')$  as integrands.

**[0062]** Appropriate interpolation functions can be found as follows. The functions should be such that yield an analytical solution to the integral in Eq. (3). In addition, because of the derivative operator in Eq. (3), the interpolation functions should also be differentiable or piecewise differentiable. Preferably, a linear interpolation is used for which the resulting function  $h_r(r)$  is piecewise planar.

**[0063]** The interpolation is performed by tiling the x-y reconstruction plane with right-angle triangles with vertexes on the grid point as exemplary illustrated in Figure 5. For each coordinate  $(x_i, y_i)$   $h_r(r_i)$  is assigned as its elevation value on the z axis, i.e.  $z_i=h_r(r_i)$ . Accordingly, each triangle can be described by a set of the three coordinates of its vertices  $(x_i, y_i, z_i)$ ,  $(x_n, y_n, z_n)$ , and  $(x_m, y_m, z_m)$ . The interpolated values of  $h_r(r)$  within each triangle are thus taken as the value of the plane elevation calculated via

$$h_r(x, y) = - \frac{Ax + By + D}{C}, \quad (7)$$

where

$$A = \begin{vmatrix} 1 & y_\ell & z_\ell \\ 1 & y_n & z_n \\ 1 & y_m & z_m \end{vmatrix}, B = \begin{vmatrix} x_\ell & 1 & z_\ell \\ x_n & 1 & z_n \\ x_m & 1 & z_m \end{vmatrix}, C = \begin{vmatrix} x_\ell & y_\ell & 1 \\ x_n & y_n & 1 \\ x_m & y_m & 1 \end{vmatrix}, D = \begin{vmatrix} x_\ell & y_\ell & z_\ell \\ x_n & y_n & z_n \\ x_m & y_m & z_m \end{vmatrix} \quad (8)$$

and the operation  $|\cdot|$  refers to matrix determinant. Substituting Eq. (7) into Eq.(4), one obtains

$$\int_{R=ct} \frac{h(r')}{R} dA' = -C^{-1} \int_{\theta_1}^{\theta_2} [A(x_0 + R \cos \theta) + B(y_0 + R \sin \theta) + D] d\theta. \quad (9)$$

5 [0064] The integral in Eq. (5) can then be solved analytically within each triangle resulting in a linear function of  $z_\rho$ ,  $z_\eta$ , and  $z_m$ . The coefficients of  $z_\rho$ ,  $z_\eta$ , and  $z_m$  are subsequently used to calculate  $g_i(r, t)$ .

10 [0065] With the example shown in Figure 6, each grid point is assigned three coordinates. Each right-angle triangle represents a unit cell in which the image is interpolated linearly. An example of a unit cell is shown in dotted lines, where the value of the OAT is determined solely by the 3D coordinates of its vertex points:  $(x_\rho, y_\rho, z_\rho)$ ,  $(x_\eta, y_\eta, z_\eta)$ , and  $(x_m, y_m, z_m)$ . The dashed curved line represents a certain arc on which the integral in Eq. (9) is calculated, and the large black grid points are the grid points that are involved in calculating the integral and correspond to the nonzero elements in Eq. (6).

15 [0066] Next, the spatial and temporal coordinates  $\{(x_j, t_j)\}_j$  are defined over which the acoustic signal is acquired. Denoting  $p_j = p(x_j, t_j)$  and  $h_j = h(x_j)$ , the following matrix equation is obtained:

$$\mathbf{p} = \mathbf{M}\mathbf{h} \quad (10)$$

where  $\mathbf{p}$  is a vector whose elements are  $p_j$ , and  $\mathbf{h}$  is a vector whose element are  $h_j$ .

20 [0067] The elements in the matrix  $\mathbf{M}$  are defined by the image grid, the measurement's spatial and temporal coordinates, and on the type of approximation being used. In particular, the elements in the matrix  $\mathbf{M}$  are the corresponding values of  $g_i(r, t)$ . Thus, for a given optoacoustic imaging system, the matrix  $\mathbf{M}$  does not depend on the imaged object, and thus can be pre-calculated before the experiment is performed.

25 [0068] When the frequency response of the acoustic detector is approximately known, it can be incorporated into the forward model. The frequency response is discretized and saved in a vector  $\mathbf{s}$ . Then a diagonal matrix  $\mathbf{M}_s$  is constructed whose diagonal elements correspond to the elements in the vector  $\mathbf{s}$ .  $\mathbf{F}$  is denoted to be the one-dimensional discrete Fourier transform matrix, i.e.  $\mathbf{F}\mathbf{p}$  is the discrete Fourier transform of  $\mathbf{p}$ . Thus, the spectrum of the measured signals  $\mathbf{p}_s$  is given by  $\mathbf{p}_s = \mathbf{M}_s\mathbf{F}\mathbf{p}$  and fulfills the equation:

$$\mathbf{p}_s = \mathbf{M}_s\mathbf{F}\mathbf{M}\mathbf{h}. \quad (11)$$

35 [0069] The optoacoustic inversion method may also include additional effects that appear in the system. If the imaged object is acoustically heterogeneous, and the sound velocity variations within the objects are known, they may be incorporated into the matrix equation. This can be achieved by recalculating the matrix  $\mathbf{M}$  for the following equation instead of Eq. 3:

$$p(x, t) \propto \frac{\partial}{\partial t} \int_{s(t)} \frac{h(x')}{R} dA' \quad (12)$$

where  $S(t)$  is a curve or surface on which every point has the same time of flight  $t$  to the detector.

45 [0070] Another effect that can be incorporated in the matrix relation may result from variations in the illumination profile for different detector locations. Such variations can appear if the object is rotated with respect to the light source and the detectors. In that case, the integral in Eq. (12) should be generalized to

$$p(x, t, \theta) \propto \frac{\partial}{\partial t} \int_{s(t, \theta)} \frac{U(x', \theta)h(x')}{R} dA', \quad (13)$$

where  $U(x', \theta)$  is an estimation to the fluence within the object for the projection at angle  $\theta$ .

55 [0071] In order to recover the optoacoustic image  $\mathbf{h}$ , Eq. (11) is inverted. Several methods exist to perform the inversion. An approach according to the invention is based on using least square error techniques. In this approach, the vector  $\mathbf{h}$  which minimizes the following square error is found:

$$\|\mathbf{p}_s - \mathbf{M}_s \mathbf{F} \mathbf{M} \mathbf{h}\|_2^2. \quad (14)$$

[0072] The minimization can be performed using standard numerical techniques such as gradient descent, conjugate gradient, LSQR, etc.. Alternatively, the minimization is performed by calculating the pseudo-inverse of the matrix  $\mathbf{M}_s \mathbf{F} \mathbf{M}$ . The advantage of using the pseudo-inverse is that it only depends on the system characteristics and not on the measured object. In this case, the reconstruction amounts to multiplying  $\mathbf{p}_s$  by a predetermined matrix. The model matrix is sparse, i.e. most of its elements are zero. This property may be used for improving the inversion process, as well as the matrix' storage.

[0073] When the measured data is insufficient for obtaining an accurate reconstruction, e.g. in the case in which some projections are unattainable, adaptive methods could be used to invert Eq. (11). As a first step, one needs to find a library in which the optoacoustic image is expected to be sparse. Once such a library is found, the optoacoustic image over the grid can be represented as  $\mathbf{h} = \mathbf{Q}\alpha$ , where  $\alpha$  is a vector containing the coefficients of the library elements, and  $\mathbf{Q}$  is the matrix defining the library elements. For a sparse representation of  $\mathbf{h}$ , most of the elements in  $\alpha$  should be close to zero. The inversion is performed by finding the sparsest signal that returns a low error for Eq. (12):

$$\min_{\alpha} \|\alpha\|_0 \quad \text{subject to} \quad \|\mathbf{p}_s - \mathbf{M}_s \mathbf{F} \mathbf{M} \mathbf{Q} \alpha\| < \varepsilon, \quad (15)$$

where  $\varepsilon$  is the acceptable reconstruction error. Methods for solving the optimization problem of Eq. (15) are described in the following section 3.

[0074] Another way to address the reconstruction problem when only partial information is available is to add a regularization term to Eq. (14), or perform singular value decomposition. The last singular values in the decomposition, which may correspond to artifacts in the reconstructed image, may be truncated or attenuated by some function of the values or their corresponding eigen-images.

[0075] Numerical simulations (implemented in Matlab, Mathworks Inc., Natick, MA, and executed on a Intel® Core™2 Quad Processors CPU operating at 2.67GHz) have been performed for testing the inventive matrix inversion method. As an example, an image with a size of some cm was reconstructed assuming a detector with a flat frequency response. The number of projections used for the inversion was 80 and the number of grid points was 80 for each axis. The temporal resolution which was used for the acoustic field was twice the corresponding spatial resolution. The run time for constructing and inverting the matrix was approximately 9 minutes. Once the inverse matrix was calculated, the reconstructed image was obtained in approximately 0.2 seconds. The matrix size was  $20240 \times 6400$  and occupied approximately 1 GB of memory. Reconstructing an OAT image, for which an exact analytical representation of the generated acoustic signals exists attained an exact reconstruction of the image. The results have been compared with those using the conventional filtered backprojection algorithm, whereby strong artifacts appeared in the back-projection, which did not occur in the inventive the model-based reconstruction. In experimental tests, the run time for constructing and inverting the model matrix was approximately one hour for the given experimental setup. After calculating the inverse, recovery of an image for each experiment took only about 1.3 seconds. The inverse matrix's dimensions were  $8281 \times 24120$  and it occupied approximately 3 GB of memory.

[0076] The optoacoustic image  $h$  reconstructed according to the above method can be further handled as the energy deposition image to be obtained. Preferably, the energy deposition image is subjected to the following decomposition.

### 3. Sparse-representation decomposition method

[0077] In order to decompose the optoacoustic image into at least two of its components, a sparse representation method is used. The underlying concept of sparse representation is that natural signals can be sparsely represented in appropriate function bases or libraries, i.e. they can be represented as a sum of a small number of elementary functions. Sparse representation techniques have been proven useful for denoising, compression and compressed sensing (see e.g. S. S. Chen et al. in "SIAM Review", Vol. 43, 2001, pp. 129-159).

[0078] The decomposition method is described in the following with exemplary reference to an image depending on the absorption coefficient and the further image component local light fluence in the object. Decomposing for separating other or further image components, like e. g. a distribution of the optical scattering coefficient or a distribution of a certain biomarker can be conducted in an analogue way.

[0079] The optoacoustic image  $h(x, y)$  is proportional to the product of the absorption coefficient  $\mu_{\alpha}(x, y)$  and local light fluence  $U(x, y)$ :  $h(x, y) \propto \mu_{\alpha}(x, y)U(x, y)$ . In order to use sparse-representation techniques, the signal should first be transformed from a product formula to a sum formula. This is achieved by taking the logarithm of the optoacoustic image:

$$\log[h(x, y)] = \log[\mu_a(x, y)] + \log[U(x, y)] + \text{Const} . \quad (16)$$

**[0080]** The functions  $\log[\mu_a(x, y)]$  and  $\log[U(x, y)]$  have very distinctive characteristics that enable extracting both of them from  $\log[h(x, y)]$ . The function  $\log[U(x, y)]$  is global and slowly varying, whereas the function  $\log[\mu_a(x, y)]$  is local and may have fast variations. The global variation of the function  $\log[U(x, y)]$  is smaller compared with the local variations of the function  $\log[\mu_a(x, y)]$ .

**[0081]** Figure 6 illustrates in an exemplary manner a 3D mesh of (a) the optoacoustic image, (b) absorption coefficient, and (c) fluence for a model object (for printing reasons shown with grey values). Figure 6 shows that the spatial properties of both the absorption coefficient, and fluence are distinguishable in the photoacoustic image. In particular, the features of both  $\log[\mu_a(x, y)]$  and  $\log[U(x, y)]$  are distinguishable in the function  $\log[h(x, y)]$ .

**[0082]** The inventive decomposition of  $\log[U(x, y)]$  is based on the assumption that two libraries  $\{\phi_n\}_n$  and  $\{\psi_n\}_n$  can be found which fulfill the following complimentary conditions:

- 1) The function  $\log[\mu_a(x, y)]$  can be sparsely represented in  $\{\phi_n\}_n$  but not in  $\{\psi_n\}_n$ .
- 2) The function  $\log[U(x, y)]$  can be sparsely represented in  $\{\psi_n\}_n$  but not in  $\{\phi_n\}_n$ .

**[0083]** These conditions will be called the sparsity conditions (or compatibility conditions) in the following. When the sparsity conditions are met, the optoacoustic image can be sparsely represented in the joint library  $\{\phi_n, \psi_m\}_{n,m}$ :

$$\log[h(x, y)] = \sum_{n=1}^N c_n \phi_n(x, y) + \sum_{m=1}^M d_m \psi_m(x, y). \quad (17)$$

**[0084]** Given the coefficients  $c_n$  and  $d_m$ ,  $\log[\mu_a(x, y)]$  and  $\log[U(x, y)]$  can be calculated using the following equations:

$$\log[\mu_a(x, y)] = \sum_{n=1}^N c_n \phi_n(x, y) \quad (18)$$

$$\log[U(x, y)] = \sum_{m=1}^M d_m \psi_m(x, y).$$

**[0085]** In order to decompose the optoacoustic image, two libraries (e.g. function bases) that fulfill the sparsity conditions are chosen.

**[0086]** For  $\log[U(x, y)]$  the 2-dimensional discrete Fourier basis is preferred. The Fourier basis is very useful for sparse representation of smooth and global functions, such as  $\log[U(x, y)]$ , but cannot be used to sparsely represent functions with local details, such as  $\log[\mu_a(x, y)]$ .

**[0087]** The problem of finding a library that can sparsely represent general images, such as  $\log[\mu_a(x, y)]$ , has been extensively studied by the signal-processing community for the past decade. One possibility is to use the 2-dimensional discrete Haar wavelet basis to represent  $\log[\mu_a(x, y)]$ . Haar wavelets are local, piecewise-constant functions and constitute the simplest library that can be used to sparsely represent natural images. It has been found that these wavelets are successful in sparsely representing images with discontinuities and are thus appropriate for representing  $\log[\mu_a(x, y)]$  in particular when the optoacoustic image is of a phantom. Haar wavelets can also be used for optoacoustic images obtained in in-vivo imaging of biological tissue. However, for such images, more complex dictionaries are preferred. The optimum library, in particular for sparsely representing natural images, can be selected in dependency on the imaging conditions and/or on the type of image being analyzed. The library may contain various distinct functions and function bases: translational variant or invariant wavelets (e.g. Haar wavelets, Daubechies wavelets, Coiflets, etc.), curvelets, contourlets, edgelets, functions obtained through a learning process, user-defined functions, etc..

**[0088]** A priori information on the nature of the problem can further improve the choice of library. For example, when the image is expected to contain blood vessels, curvelets may be added to the library of the absorption coefficient, as they can sparsely represent one-dimensional curves. In addition functions can be defined manually or automatically according to the properties of the image. When the objects with well defined boundary appear in the image, one can detect the boundaries (manually or automatically) and assign a function that accepts a constant within the boundaries and zero outside them. These functions can also be added to the library of the absorption coefficient. One can also add elements to the library representing the light fluence. The inverse of the zero-th order modified Bessel function, which

describes 2D propagation of light in scattering media, can be added:  $1/I_0(\kappa|\vec{r} - \vec{a}|)$ . Several values of  $\kappa$  or  $\vec{a}$  may be chosen corresponding to different attenuation rates and minimum fluence positions, respectively.

[0089] Because the decomposition is based on distinguishing between local and global properties, the background value of the absorption coefficient cannot be extracted. Thus, the reconstruction of  $\log[\mu_a(x,y)]$  is accurate up to an additive constant and the reconstruction of  $\mu_a(x,y)$  is correct up to scaling. In order to scale an absorption coefficient that is obtained in an experiment, the experimental setup is calibrated. One way of doing so is by estimating the illumination on the surface of the object. This can be used to find  $\mu_a(x,y)$  on the surface and recover the scaling factor. Another way would be to use a phantom with a known absorption in order to calibrate the system.

[0090] Figure 7 illustrates in an exemplary manner that the combination of the Fourier and Haar bases fulfill the sparsity conditions. In the example, the functions were scaled to match the functions in Figure 6. Figures 7a and 7b show the functions  $\log[\mu_a(x; y)]$  and  $\log[U(x; y)]$  (discretized and represented on a grid) calculated with only 200 and 100 elements respectively. The figure clearly shows that both functions can be sparsely represented in their respective bases. In Figs. 7c and 7d the two functions are represented with the opposite bases and increased the number of elements to 250. The figure clearly shows that in spite of the increased number of elements, the functions were not well represented in the opposite bases.

[0091] Once two libraries that fulfill the sparsity condition are chosen, the decomposition problem is to find the minimum number of coefficients  $c_n$  and  $d_m$  that fulfill Eq. (17). In its discrete version the decomposition problem can be written in matrix form:

$$\min_{\alpha} \|\alpha\|_0 \quad \text{subject to} \quad h = \mathbf{A} \alpha \quad (19)$$

where  $\alpha$  is a column vector whose elements are  $c_n$  and  $d_m$ ,  $\alpha = [c_1, \dots, c_n, d_1, \dots, d_m]$ ;  $h$  is a column vector with  $\log(h_k)$  as elements; and  $\mathbf{A}$  is a  $K$  by  $(N+M)$  matrix whose columns correspond to the library functions  $\phi_{n,k}$  and  $\psi_{n,k}$ . The zero norm  $\|\cdot\|_0$  is the number of nonzero elements in a given vector. Because in practical cases, Eqs. (17) and (18) are mere approximations, Eq. (19) should be replaced by

$$\min_{\alpha} \|\alpha\|_0 \quad \text{subject to} \quad \|x - \mathbf{A} \alpha\| < \varepsilon, \quad (20)$$

where  $\varepsilon$  is the acceptable reconstruction error.

[0092] The optimization problem in Eq. (20) is non-convex, and generally can only be solved with non-polynomial complexity. Two notable methods to approximate the solution of Eq. (20) are the basis-pursuit and matching-pursuit algorithms. Basis pursuit is based on replacing the zero norm in Eq. (20) with the  $\ell_1$  norm. In the  $\ell_1$  norm, the problem is convex, and can be solved more efficiently than the zero-norm problem using linear programming. It has been shown that when the representation is sufficiently sparse, the results obtained by both norms are identical. Matching pursuit (MP) is an iterative algorithm for solving Eqs. (19) and (20). In MP, one iteratively builds the image from the elements of the original library. In each step, one element from the library is added to the representation of the image. The iterations stop once the signal is represented with sufficient accuracy or when the number of iterations has been exceeded. A variation of MP, called orthogonal matching pursuit (OMP) may also be used.

[0093] The main difference between the two MP algorithms is in the way in which the coefficients for the chosen library elements are calculated. In standard MP, the coefficient of each library element is chosen only once - when the element is added to the signal representation. Thus, errors in any of the iterative steps cannot be corrected in the further iterations. In OMP, the optimal coefficients for all the elements are recalculate for each iterations, thus allowing compensation for errors in early iterations.

[0094] After Eq. (20) has been solved, a solution vector  $\alpha_l$  ( $l$  indicating the size of the vector) is obtained in which most elements are equal to zero (or are very close to zero), and a reduced matrix  $\mathbf{A}_l$  is obtained which contains only those rows of  $\mathbf{A}$  which correspond to the nonzero elements in  $\alpha_l$ .

[0095] From the matrix  $\mathbf{A}_l$ , two new matrices  $\mathbf{B}$  and  $\mathbf{C}$  are constructed. The matrices  $\mathbf{B}$  and  $\mathbf{C}$  are composed out of the columns of  $\mathbf{A}_l$  corresponding to the absorption coefficient basis  $\{\phi_n\}_n$  and fluence basis  $\{\psi_n\}_n$ , respectively. Accordingly, two vectors  $\beta$  and  $\gamma$  are constructed out of  $\alpha_l$ . The vector representation of  $\log[\mu_a(x,y)]$  and,  $\log[U(x,y)]$  denoted by  $\mathbf{b}$  and  $\mathbf{c}$  respectively, is calculated using the following equations:

$$\begin{aligned} \mathbf{b} &= \mathbf{B}\beta \\ \mathbf{c} &= \mathbf{C}\gamma \end{aligned} \quad (21)$$

[0096] The local absorption coefficient image  $\mu$  reconstructed according to the above method can be further processed with conventional image processing or data handling techniques.

[0097] Numerical simulations conducted with examples like in Figure 7 and with a more complex-shaped absorption coefficient image have proved that the inventive reconstruction is capable to recover the absorption coefficient image of the object even if the model data are superimposed with noise data. Furthermore, the method was successfully tested in experiment with a tissue-mimicking phantom, resembling typical small-animal whole-body imaging configuration and the corresponding tissue properties and other experimental parameters.

#### 4. Normalization and application to MSOT

[0098] When optoacoustic images are taken for different excitation wavelengths, the decomposition may be applied not only to the images themselves, but also to normalized differences and/or ratios between different images and their combinations. For example, if two optoacoustic images  $h_1$  and  $h_2$  were acquired at two different illumination wavelength, one can denote their difference by  $dh$  and their sum by  $h$ . Assuming  $dh \ll h$ , the following relation is obtained:

$$dh = (d\mu)U + (dU)\mu \quad (22).$$

[0099] Equation (22) shows that the differential optoacoustic image depends both on the average fluence as well as on the change in fluence. Normalizing the differential image by the average image results in:

$$\frac{dh}{h} = \frac{d\mu}{\mu} + \frac{dU}{U}. \quad (23)$$

[0100] The normalized differential image is a sum of two distinct images: one of the absorption coefficients and one of the light fluences. As a result, the same argument that allowed the decomposition of single optoacoustic images applies also here. By using the decomposition algorithm on  $dh/h$ , both  $d\mu/\mu$  and  $dU/U$  can be extracted. Since  $\mu$  and  $U$  can be obtained from decomposing the original optoacoustic images, they can be used to finally obtain  $d\mu$  and  $dU$ . Eq. (23) can be written in an alternative logarithmic form:

$$d \log h = d \log \mu + d \log U. \quad (24).$$

The same analysis can be used for both forms.

[0101] The ability to accurately extract changes in the absorption coefficient allows for spectral fitting to be performed, which can be used to calculate the concentration of various substances with spectrally varying absorption coefficient. Given a set of optoacoustic images  $h_1, h_2, \dots, h_n$ , obtained for consecutive wavelengths  $\lambda_1, \lambda_2, \dots, \lambda_n$ , the differential absorption coefficients  $d\mu_1 = \mu_1 - \mu_2, \dots, d\mu_{n-1} = \mu_{n-1} - \mu_n$  can be calculated using the process described above. The set  $\{d\mu_1, d\mu_2, \dots, d\mu_{n-1}\}$  together with the absorption coefficient at any other of the measurement's wavelengths, uniquely determines the set of absorption coefficients for all the measured wavelengths  $\{\mu_1, \mu_2, \dots, \mu_n\}$ . Each of the two sets, or any of their processed versions, can be used as input for spectral fitting algorithms that determine the concentration of different substances according to their absorption spectrum. The spectral fitting can be obtained by minimizing the following square error:

$$\sum_{n'=1}^n \left| \sum_{k'=1}^k \eta_{k'} S_{k'}(\lambda_{n'}) - \mu_{n'} \right|^2 \quad (25)$$

where  $\eta_{k'}$  is the concentration of substance  $k'$  and  $S_{k'}(\lambda_{n'})$  is its absorption spectrum for the wavelength  $\lambda_{n'}$ . The spectral

fitting can be performed by other methods known in the prior art, such as principle components analysis, independent component analysis or other types of source separation. The sparsity of the images may also be used in the fitting.

## 5. Preferred system features

**[0102]** Figure 8 schematically illustrates further configuration details of the image reconstruction device 22 conducting the inventive optoacoustic inversion method (see section 2.). The image reconstruction device 22 comprises a first input device 221 receiving pressure signals from the signal collecting device 10 (see Figure 1), at least one second input device 222, 223 receiving measurement conditions for adjusting the propagation matrix, a matrix adjustment circuit 224, an optoacoustic inversion circuit 225, and an image data output 226. The optoacoustic inversion circuit 225 is configured for implementing the above inversion of equation (11) e. g. based on the minimization of equation (14). Integration of the matrix adjustment circuit 225 into the image reconstruction device 22 is not strictly necessary. The propagation matrix can be pre-calculated separately and input to the optoacoustic inversion circuit 224 without additional adjustment.

**[0103]** As mentioned above, the reconstruction of the energy deposition image comprises a numerical method, e. g. an iterative propagation model based simulation. Figure 9 schematically illustrates a correspondingly adapted embodiment of the image reconstruction device 22, which comprises an input device 221 receiving pressure signals from the signal collecting device 10 (see Figure 1), a start model adjustment circuit 227, a propagation model simulation circuit 228, and an image data output 226. The propagation model simulation circuit 228 is configured for implementing the iterative propagation model based simulation of the pressure signals.

**[0104]** According to Figure 10, the absorption image decomposition device 23 conducting the inventive decomposition method (see section 3) comprises an energy deposition image data input 231, a logarithm circuit 232, a library coefficient optimization circuit 233 and first and second outputs 236, 237 delivering the decomposed image components comprising the absorption coefficient image and e. g. the fluence image, resp.. The library coefficient optimization circuit 233 is connected with a local library selection circuit 234 and a global library selection circuit 235.

**[0105]** The features of the invention in the above description, the drawings and the claims can be of significance both individually as well in combination for the realisation of the invention in its various embodiments.

## Claims

### 1. Method of thermoacoustic imaging, comprising the steps of:

- pre-calculating a forward model matrix  $M$  representing a relation between an amount of electromagnetic energy absorbed in an object and thermoacoustic signals produced in response to a delivery of electromagnetic energy into the object, wherein the following matrix equation is fulfilled:  $p=Mh$ , wherein  $h$  is a vector having elements  $h_i$  that correspond to amounts of electromagnetic energy absorbed at coordinates  $x_i$  in the object and  $p$  is a vector having elements  $p_j$  corresponding to thermoacoustic signals at coordinates  $x_j$  and at times  $t_j$ ,
- delivering electromagnetic energy to the object,
- recording thermoacoustic signals ( $p(x_j, t_j)$ ) representing a mechanical wave response to the delivery of electromagnetic energy to the object, and
- reconstructing an energy deposition image representing a local energy deposition within the object based on the recorded thermoacoustic signals ( $p(x_j, t_j)$ ), said reconstructing step including inverting the matrix equation  $p=Mh$  to recover the energy deposition image by
  - calculating a pseudo-inverse of the forward model matrix  $M$  and multiplying the pseudo-inverse of the forward model matrix  $M$  with the vector containing the recorded thermoacoustic signals ( $p(x_j, t_j)$ ), or
  - least square error minimization of the matrix equation  $p=Mh$ , wherein the vector  $p$  contains the recorded thermoacoustic signals ( $p(x_j, t_j)$ ).

### 2. The imaging method according to claim 1, wherein

- the model matrix depends on a geometry of collecting the thermoacoustic signals, and/or
- the model matrix is adjusted in dependency on at least one of an acoustic heterogeneity of the object, a geometric profile of the illumination of the imaged object by the light pulses, and a frequency response of a detector device utilized for collecting the thermoacoustic signals.

### 3. The imaging method according to one of the foregoing claims, comprising the steps of decomposing the energy deposition image into a quantitative absorption image representing a distribution of a local absorption coefficient in

the object and at least one further image component.

4. The imaging method according to claim 3, wherein the thermoacoustic signals represent a mechanical wave response to a delivery of light pulses, which have at least one illumination wavelength and at least one polarization state.

5. The imaging method according to claim 4, wherein:

- the energy deposition image is reconstructed based on the thermoacoustic signals acquired at the at least one illumination wavelength and/or the at least one light polarization,
- multiple energy deposition images are separately reconstructed based on the thermoacoustic signals acquired at the different illumination wavelengths and/or the different light polarizations, or
- the energy deposition image is reconstructed based on a combination of the thermoacoustic signals acquired at the different illumination wavelengths and/or the different light polarizations, wherein the combination comprises linear or nonlinear combinations of signals.

6. The imaging method according to one of the foregoing claims, wherein the inverted model matrix approach further includes at least one of a singular value decomposition and an algebraic reconstruction technique (ART).

7. The imaging method according to claim 6, wherein

- the model matrix depends on the geometry of a detector device collecting the thermoacoustic signals, and/or
- the model matrix is adjusted in dependency on at least one of an acoustic heterogeneity of the object, a geometric profile of the delivered electromagnetic energy in the imaged object, a frequency response of a detector device utilized for collecting the thermoacoustic signals and a result of the decomposing step.

8. The imaging method according to one of the claims 3 to 7, wherein the energy deposition image decomposing step comprises providing a logarithmic representation of the energy deposition image, and calculating the quantitative absorption image and the at least one further image component as summands of the logarithmic representation.

9. The imaging method according to one of the claims 3 to 8, wherein the at least one further image component comprises at least one of an excitation light fluence distribution image, a distribution of speed of sound, an electric or magnetic field distribution, a dielectric constant distribution, a thermoelastic expansion coefficient distribution, and a heat capacity distribution.

10. Imaging device for optoacoustic imaging of an object, comprising:

- a matrix storage configured to store a forward model matrix  $M$  and/or its inverse, the forward model matrix representing a relation between an amount of electromagnetic energy absorbed in an object and thermoacoustic signals produced in response to a delivery of electromagnetic energy into the object, wherein the following matrix equation is fulfilled:  $p=Mh$ , wherein  $h$  is a vector having elements  $h_i$  that correspond to amounts of electromagnetic energy absorbed at coordinates  $x_i$  in the object and  $p$  is a vector having elements  $p_j$  corresponding to thermoacoustic signals at coordinates  $x_j$  and at times  $t_j$ ,
- a signal collecting device comprising an electromagnetic energy source and an acoustic signal recording device including at least one acoustic detection element and being adapted for recording thermoacoustic signals  $(p(x_j, t_j))$  representing a mechanical wave response to a delivery of electromagnetic energy into the imaged object, and
- an energy-deposition image reconstruction device being adapted for reconstructing an energy deposition image representing a local energy deposition within the object based on the recorded thermoacoustic signals  $(p(x_j, t_j))$ , wherein the energy deposition image reconstruction device comprises an inversion circuit being adapted for subjecting the thermoacoustic signals  $(p(x_j, t_j))$  to a matrix-based acoustic inversion utilizing an inverted model matrix approach, wherein the matrix equation  $p=Mh$  is inverted to recover the energy deposition image by
  - calculating a pseudo-inverse of the forward model matrix  $M$  and multiplying the pseudo-inverse of the forward model matrix  $M$  with the vector containing the recorded thermoacoustic signals  $(p(x_j, t_j))$ , or
  - least square error minimization of the matrix equation  $p=Mh$ , wherein the vector  $p$  contains the recorded thermoacoustic signals  $(p(x_j, t_j))$ .

11. The imaging device according to claim 10, wherein the inversion circuit includes the matrix storage.

12. The imaging device according to one of the claims 10 to 11, further comprising an absorption image decomposition device being adapted for decomposing the energy deposition image into a quantitative absorption image representing a distribution of a local absorption coefficient in the object and at least one further image component.
- 5 13. The imaging device according to one of the claims 10 to 12, wherein the inversion circuit includes an adjustment device being adapted for adjusting the model matrix in dependency on at least one of an acoustic heterogeneity of the object, a geometric profile of the illumination of the imaged object by the light pulses, a frequency response of a detector device utilized for collecting the thermoacoustic signals and an output of the decomposition device.
- 10 14. Computer program residing on a computer-readable medium, with a program code for carrying out the method according to at least one of the claims 1 to 9.
15. Apparatus comprising a computer-readable storage medium containing program instructions for carrying out the method according to at least one of the claims 1 to 9.

15

### Patentansprüche

- 20 1. Thermoakustisches Bildgebungsverfahren, das die folgenden Schritte umfasst:
- Vorberechnen einer Vorwärtsmodellmatrix  $M$ , die ein Verhältnis zwischen einer Menge in einem Objekt absorbiertes elektromagnetischer Energie und thermoakustischen Signalen, die als Reaktion auf eine Zufuhr elektromagnetischer Energie in das Objekt erzeugt werden, darstellt, wobei die nachstehende Matrixgleichung erfüllt wird:  $p=Mh$ , wobei  $h$  ein Vektor mit Elementen  $h_i$  ist, die Mengen elektromagnetischer Energie entsprechen, die an Koordinaten  $x_i$  im Objekt absorbiert sind, und  $p$  ein Vektor mit Elementen  $p_j$  ist, die thermoakustischen Signalen an Koordinaten  $x_j$  und Zeitpunkten  $t_j$  entsprechen,
  - Zufuhr elektromagnetischer Energie in das Objekt,
  - Aufzeichnung thermoakustischer Signale ( $p(x_j, t_j)$ ), die eine Reaktion auf die Zufuhr elektromagnetischer Energie in das Objekt in Form einer mechanischen Welle darstellen, und
  - 30 - Rekonstruieren eines Energiedepositionsbildes, das eine örtliche Energiedeposition im Objekt darstellt, auf Basis der aufgezeichneten thermoakustischen Signale ( $p(x_j, t_j)$ ), wobei im Rekonstruktionsschritt die Matrixgleichung  $p=Mh$  invertiert wird, um das Energiedepositionsbild zu erhalten, indem
    - 35 - eine Pseudoinverse der Vorwärtsmodellmatrix  $M$  berechnet und die Pseudoinverse der Vorwärtsmodellmatrix  $M$  mit dem die aufgezeichneten thermoakustischen Signale ( $p(x_j, t_j)$ ) enthaltenden Vektor multipliziert wird, oder
    - eine Minimierung der kleinsten Fehlerquadrate der Matrixgleichung  $p=Mh$  durchgeführt wird, wobei der Vektor  $p$  die aufgezeichneten thermoakustischen Signale ( $p(x_j, t_j)$ ) enthält.
- 40 2. Bildgebungsverfahren nach Anspruch 1, wobei
- die Modellmatrix von einer Geometrie des Sammelns der thermoakustischen Signale abhängt, und/oder
  - die Modellmatrix in Abhängigkeit von einer akustischen Heterogenität des Objekts und/oder einem geometrischen Profil der Beleuchtung des abgebildeten Objekts durch die Lichtimpulse und/oder einer Frequenzabhängigkeit einer zum Sammeln der thermoakustischen Signale eingesetzten Detektorvorrichtung angepasst wird.
- 45 3. Bildgebungsverfahren nach einem der vorangehenden Ansprüche, umfassend die Schritte der Zerlegung des Energiedepositionsbildes in ein quantitatives Absorptionsbild, das eine Verteilung eines örtlichen Absorptionskoeffizienten im Objekt darstellt, und mindestens eine weitere Bildkomponente.
- 50 4. Bildgebungsverfahren nach Anspruch 3, wobei die thermoakustischen Signale eine Reaktion in Form einer mechanischen Welle auf die Zufuhr von Lichtimpulsen, die mindestens eine Beleuchtungswellenlänge und mindestens einen Polarisationszustand aufweisen, darstellen.
- 55 5. Bildgebungsverfahren nach Anspruch 4, wobei
- das Energiedepositionsbild auf Basis der thermoakustischen Signale, die bei der mindestens einer Beleuchtungswellenlänge und/oder der mindestens einen Lichtpolarisation erfasst werden, rekonstruiert wird,

- mehrere Energiedepositionsbilder auf Basis der thermoakustischen Signale, die bei den unterschiedlichen Beleuchtungswellenlängen und/oder den unterschiedlichen Lichtpolarisationen erfasst werden, getrennt rekonstruiert werden, oder
  - das Energiedepositionsbild auf Basis einer Kombination der thermoakustischen Signale, die bei den unterschiedlichen Beleuchtungswellenlängen und/oder den unterschiedlichen Lichtpolarisationen erfasst werden, rekonstruiert wird, wobei die Kombination lineare oder nicht-lineare Kombinationen von Signalen umfasst.
- 5
6. Bildgebungsverfahren nach einem der vorangehenden Ansprüche, wobei der Ansatz mit invertierter Modellmatrix ferner eine Singulärwertzerlegung und/oder eine algebraische Rekonstruktionstechnik (ART) umfasst.
- 10
7. Bildgebungsverfahren nach Anspruch 6, wobei
- die Modellmatrix von der Geometrie einer die thermoakustischen Signale sammelnden Detektorvorrichtung abhängt, und/oder
  - die Modellmatrix in Abhängigkeit von einer akustischen Heterogenität des Objekts und/oder einem geometrischen Profil der dem abgebildeten Objekt zugeführten elektromagnetischen Energie und/oder einer Frequenzabhängigkeit einer zum Sammeln der thermoakustischen Signale eingesetzten Detektorvorrichtung und/oder einem Ergebnis des Zerlegungsschritts angepasst wird.
- 15
8. Bildgebungsverfahren nach einem der Ansprüche 3 bis 7, wobei im Schritt des Zerlegens des Energiedepositionsbildes eine logarithmische Darstellung des Energiedepositionsbildes vorgenommen wird und das quantitative Absorptionsbild und die mindestens eine weitere Bildkomponente als Summanden der logarithmischen Darstellung berechnet werden.
- 20
9. Bildgebungsverfahren nach einem der Ansprüche 3 bis 8, wobei die mindestens eine weitere Bildkomponente ein Anregungslichtflussverteilungsbild und/oder eine Verteilung der Schallgeschwindigkeit und/oder eine Verteilung eines elektrischen oder magnetischen Feldes und/oder eine Verteilung einer dielektrischen Konstante und/oder eine Verteilung eines thermoelastischen Ausdehnungskoeffizienten und/oder eine Verteilung einer Wärmekapazität umfasst.
- 25
10. Bildgebungsapparatur für optoakustische Bildgebung eines Objekts, umfassend:
- einen Matrixspeicher, der so konfiguriert ist, dass eine Vorwärtsmodellmatrix  $M$  und/oder ihre Inverse gespeichert wird bzw. werden, wobei die Vorwärtsmodellmatrix ein Verhältnis zwischen einer Menge in einem Objekt absorbiertener elektromagnetischer Energie und thermoakustischen Signalen, die als Reaktion auf eine Zufuhr elektromagnetischer Energie in das Objekt erzeugt werden, darstellt, wobei die nachstehende Matrixgleichung erfüllt wird:  $p=Mh$ , wobei  $h$  ein Vektor mit Elementen  $h_i$  ist, die Mengen elektromagnetischer Energie entsprechen, die an Koordinaten  $x_i$  im Objekt absorbiert sind, und  $p$  ein Vektor mit Elementen  $p_j$  ist, die thermoakustischen Signalen an Koordinaten  $x_j$  und Zeitpunkten  $t_j$  entsprechen,
  - eine Signalsammelvorrichtung, umfassend eine elektromagnetische Energiequelle und eine Vorrichtung zur Aufzeichnung akustischer Signale, die mindestens ein akustisches Detektionselement umfasst und zur Aufzeichnung thermoakustischer Signale ( $p(x_j, t_j)$ ) angepasst ist, die eine Reaktion auf eine Zufuhr elektromagnetischer Energie in das abgebildete Objekt in Form einer mechanischen Welle darstellen, und
  - eine Vorrichtung zum Rekonstruieren eines Energiedepositionsbildes, die zum Rekonstruieren eines Energiedepositionsbildes angepasst ist, das eine örtliche Energiedeposition im Objekt auf Basis der aufgezeichneten thermoakustischen Signale ( $p(x_j, t_j)$ ) darstellt, wobei die Vorrichtung zum Rekonstruieren eines Energiedepositionsbildes eine Inversionsschaltung umfasst, die so angepasst ist, dass sie die thermoakustischen Signale ( $p(x_j, t_j)$ ) unter Anwendung eines Ansatzes mit invertierter Modellmatrix einer matrixbasierten akustischen Inversion unterzieht, wobei die Matrixgleichung  $p=Mh$  invertiert wird, um das Energiedepositionsbild zu erhalten, indem
  - eine Pseudoinverse der Vorwärtsmodellmatrix  $M$  berechnet und die Pseudoinverse der Vorwärtsmodellmatrix  $M$  mit dem die aufgezeichneten thermoakustischen Signale ( $p(x_j, t_j)$ ) enthaltenden Vektor multipliziert wird, oder
  - eine Minimierung der kleinsten Fehlerquadrate der Matrixgleichung  $p=Mh$  durchgeführt wird, wobei der Vektor  $p$  die aufgezeichneten thermoakustischen Signale ( $p(x_j, t_j)$ ) enthält.
- 30
- 35
- 40
- 45
- 50
- 55
11. Bildgebungsapparatur nach Anspruch 10, wobei die Inversionsschaltung den Matrixspeicher umfasst.
12. Bildgebungsapparatur nach einem der Ansprüche 10 bis 11, die ferner eine Vorrichtung zum Zerlegen eines

Absorptionsbildes umfasst, die zum Zerlegen des Energiedepositionsbildes in ein quantitatives Absorptionsbild, das eine Verteilung eines örtlichen Absorptionskoeffizienten im Objekt darstellt, und mindestens eine weitere Bildkomponente angepasst ist.

- 5 13. Bildgebungsvorrichtung nach einem der Ansprüche 10 bis 12, wobei die Inversionsschaltung eine Einstellvorrichtung umfasst, die so angepasst ist, dass sie die Modellmatrix in Abhängigkeit von einer akustischen Heterogenität des Objekts und/oder einem geometrischen Profil der Beleuchtung des abgebildeten Objekts durch die Lichtimpulse und/oder einer Frequenzabhängigkeit einer zum Sammeln der thermoakustischen Signale eingesetzten Detektorvorrichtung und/oder einer Ausgabe der Zerlegungsvorrichtung anpasst.
- 10 14. Computerprogramm, enthalten in einem computerlesbaren Medium, mit einem Programmcode zum Ausführen des Verfahrens nach mindestens einem der Ansprüche 1 bis 9.
- 15 15. Apparat, umfassend ein computerlesbares Speichermedium, enthaltend Programmanweisungen zum Ausführen des Verfahrens nach mindestens einem der Ansprüche 1 bis 9.

## Revendications

- 20 1. Procédé d'imagerie thermoacoustique comprenant les étapes consistant à:
- précalculer une matrice de modèle direct  $M$  représentant un rapport entre une quantité d'énergie électromagnétique absorbée dans un objet et des signaux thermoacoustiques générés en réponse à une alimentation d'énergie électromagnétique dans ledit objet, l'équation de matrice reprise ci-après étant satisfaite:  $p=Mh$ , où  $h$  représente un vecteur comprenant des éléments  $h_i$  correspondant à des quantités d'énergie électromagnétique absorbées à des coordonnées  $x_i$  dans ledit objet et  $p$  représente un vecteur comprenant des éléments  $p_j$  correspondant à des signaux thermoacoustiques à des coordonnées  $x_j$  et des temps  $t_j$ ,
  - alimenter de l'énergie électromagnétique dans ledit objet,
  - enregistrer des signaux thermoacoustiques  $(p(x_j, t_j))$  représentant une réponse d'onde mécanique à l'alimentation d'énergie électromagnétique dans ledit objet, et
  - reconstruire une image de dépôt d'énergie représentant un dépôt d'énergie local dans ledit objet sur base des signaux thermoacoustiques  $(p(x_j, t_j))$  enregistrés, l'étape de reconstruction comprenant l'inversion de l'équation de matrice  $p=Mh$  afin de récupérer l'image de dépôt d'énergie
- en calculant un pseudo-inverse de la matrice de modèle direct  $M$  et en multipliant le pseudo-inverse de la matrice de modèle direct  $M$  avec le vecteur comprenant les signaux thermoacoustiques  $(p(x_j, t_j))$  enregistrés, ou
  - en effectuant une minimisation des erreurs des moindres carrés de l'équation de matrice  $p=Mh$ , où le vecteur  $p$  comprend les signaux thermoacoustiques  $(p(x_j, t_j))$  enregistrés.
- 40 2. Procédé d'imagerie selon la revendication 1, **caractérisé en ce que**
- la matrice de modèle dépend d'une géométrie de collection des signaux thermoacoustiques, et/ou
  - la matrice de modèle est adaptée en fonction d'une hétérogénéité acoustique de l'objet et/ou d'un profil géométrique de l'irradiation de l'objet imagé par les impulsions lumineuses et/ou d'une réponse de fréquence d'un dispositif de détecteur utilisé pour la collection des signaux thermoacoustiques.
- 50 3. Procédé d'imagerie selon l'une quelconque des revendications précédentes, comprenant les étapes de la décomposition de l'image de dépôt d'énergie en une image d'absorption quantitative représentant une distribution d'un coefficient d'absorption locale dans ledit objet et au moins une autre composante d'image.
- 55 4. Procédé d'imagerie selon la revendication 3, **caractérisé en ce que** les signaux thermoacoustiques représentent une réponse d'onde mécanique à une application d'impulsions lumineuses présentant au moins une longueur d'onde d'irradiation et au moins un état de polarisation.
5. Procédé d'imagerie selon la revendication 4, **caractérisé en ce que**
- l'image de dépôt d'énergie est reconstruite sur base des signaux thermoacoustiques acquis à ladite au moins

une longueur d'onde d'irradiation et/ou à ladite au moins une polarisation lumineuse,

- plusieurs images de dépôt d'énergie sont reconstruites séparément sur base des signaux thermoacoustiques acquis aux différentes longueurs d'onde d'irradiation et/ou aux différentes polarisations lumineuses, ou

- l'image de dépôt d'énergie est reconstruite sur base d'une combinaison des signaux thermoacoustiques acquis aux différentes longueurs d'onde d'irradiation et/ou aux différentes polarisations lumineuses, ladite combinaison comprenant des combinaisons linéaires ou non linéaires de signaux.

6. Procédé d'imagerie selon l'une quelconque des revendications précédentes, **caractérisé en ce que** l'approche à matrice de modèle inversée comprend en outre une décomposition en valeurs singulières et/ou une technique de reconstruction algébrique (ART).

7. Procédé d'imagerie selon la revendication 6, **caractérisé en ce que**

- la matrice de modèle dépend de la géométrie d'un dispositif de détecteur servant à la collection des signaux thermoacoustiques, et/ou

- la matrice de modèle est adaptée en fonction d'une hétérogénéité acoustique de l'objet et/ou d'un profil géométrique de l'énergie électromagnétique introduite dans l'objet imagé et/ou d'une réponse de fréquence d'un dispositif de détecteur utilisé pour la collection des signaux thermoacoustiques et/ou d'un résultat de l'étape de décomposition.

8. Procédé d'imagerie selon l'une quelconque des revendications 3 à 7, **caractérisé en ce que** l'étape de décomposition de l'image de dépôt d'énergie comprend la génération d'une représentation logarithmique de l'image de dépôt d'énergie et le calcul de l'image d'absorption quantitative et de ladite au moins une autre composante d'image comme les termes de la somme de la représentation logarithmique.

9. Procédé d'imagerie selon l'une quelconque des revendications 3 à 8, **caractérisé en ce que** ladite au moins une autre composante d'image comprend une image de distribution de fluence de lumière de stimulation et/ou une distribution de vitesse du son et/ou une distribution d'un champ électrique ou magnétique et/ou une distribution d'une constante diélectrique et/ou une distribution d'un coefficient de dilatation thermoélastique et/ou une distribution d'une capacité thermique.

10. Dispositif d'imagerie pour l'imagerie optoacoustique d'un objet, comprenant:

- une mémoire de matrice configurée de façon à ce qu'une matrice de modèle direct  $M$  et/ou son inverse soi(en)t mémorisé(e)(s), ladite matrice de modèle direct représentant un rapport entre une quantité d'énergie électromagnétique absorbée dans un objet et des signaux thermoacoustiques générés en réponse à une alimentation d'énergie électromagnétique dans ledit objet, l'équation de matrice reprise ci-après étant satisfaite:  $p=Mh$ , où  $h$  représente un vecteur comprenant des éléments  $h_i$  correspondant à des quantités d'énergie électromagnétique absorbées à des coordonnées  $x_i$  dans ledit objet et  $p$  représente un vecteur comprenant des éléments  $p_j$  correspondant à des signaux thermoacoustiques à des coordonnées  $x_j$  et des temps  $t_j$ ,

- un dispositif de collection de signaux comprenant une source d'énergie électromagnétique et un dispositif d'enregistrement de signaux acoustiques comprenant au moins un élément de détection acoustique et adapté de façon à assurer l'enregistrement de signaux thermoacoustiques  $(p(x_j, t_j))$  représentant une réponse d'onde mécanique à une alimentation d'énergie électromagnétique dans ledit objet imagé, et

- un dispositif de reconstruction d'une image de dépôt d'énergie adapté de façon à assurer la reconstruction d'une image de dépôt d'énergie représentant un dépôt d'énergie local dans ledit objet sur base des signaux thermoacoustiques  $(p(x_j, t_j))$  enregistrés, ledit dispositif de reconstruction d'une image de dépôt d'énergie comprenant un circuit d'inversion adapté de façon à soumettre les signaux thermoacoustiques  $(p(x_j, t_j))$  à une inversion acoustique basée sur une matrice en appliquant une approche à matrice de modèle inversée, l'équation de matrice  $p=Mh$  étant inversée afin de récupérer l'image de dépôt d'énergie

- en calculant un pseudo-inverse de la matrice de modèle direct  $M$  et en multipliant le pseudo-inverse de la matrice de modèle direct  $M$  avec le vecteur comprenant les signaux thermoacoustiques  $(p(x_j, t_j))$  enregistrés, ou

- en effectuant une minimisation des erreurs des moindres carrés de l'équation de matrice  $p=Mh$ , où le vecteur  $p$  comprend les signaux thermoacoustiques  $(p(x_j, t_j))$  enregistrés.

11. Dispositif d'imagerie selon la revendication 10, **caractérisé en ce que** le circuit d'inversion comprend la mémoire

de matrice.

- 5
12. Dispositif d'imagerie selon l'une quelconque des revendications 10 à 11, comprenant en outre un dispositif de décomposition d'une image d'absorption adapté de façon à assurer la décomposition de l'image de dépôt d'énergie en une image d'absorption quantitative représentant une distribution d'un coefficient d'absorption locale dans ledit objet et au moins une autre composante d'image.
- 10
13. Dispositif d'imagerie selon l'une quelconque des revendications 10 à 12, **caractérisé en ce que** le circuit d'inversion comprend un dispositif de réglage adapté de façon à adapter la matrice de modèle en fonction d'une hétérogénéité acoustique de l'objet et/ou d'un profil géométrique de l'irradiation de l'objet imagé par les impulsions lumineuses et/ou d'une réponse de fréquence d'un dispositif de détecteur utilisé pour la collection des signaux thermoacoustiques et/ou d'une sortie du dispositif de décomposition.
- 15
14. Programme informatique contenu dans un support lisible par ordinateur et comprenant un code informatique assurant l'exécution du procédé selon au moins l'une quelconque des revendications 1 à 9.
- 20
15. Appareil comprenant un support de mémoire lisible par ordinateur, comprenant des instructions de programme assurant l'exécution du procédé selon au moins l'une quelconque des revendications 1 à 9.

20

25

30

35

40

45

50

55

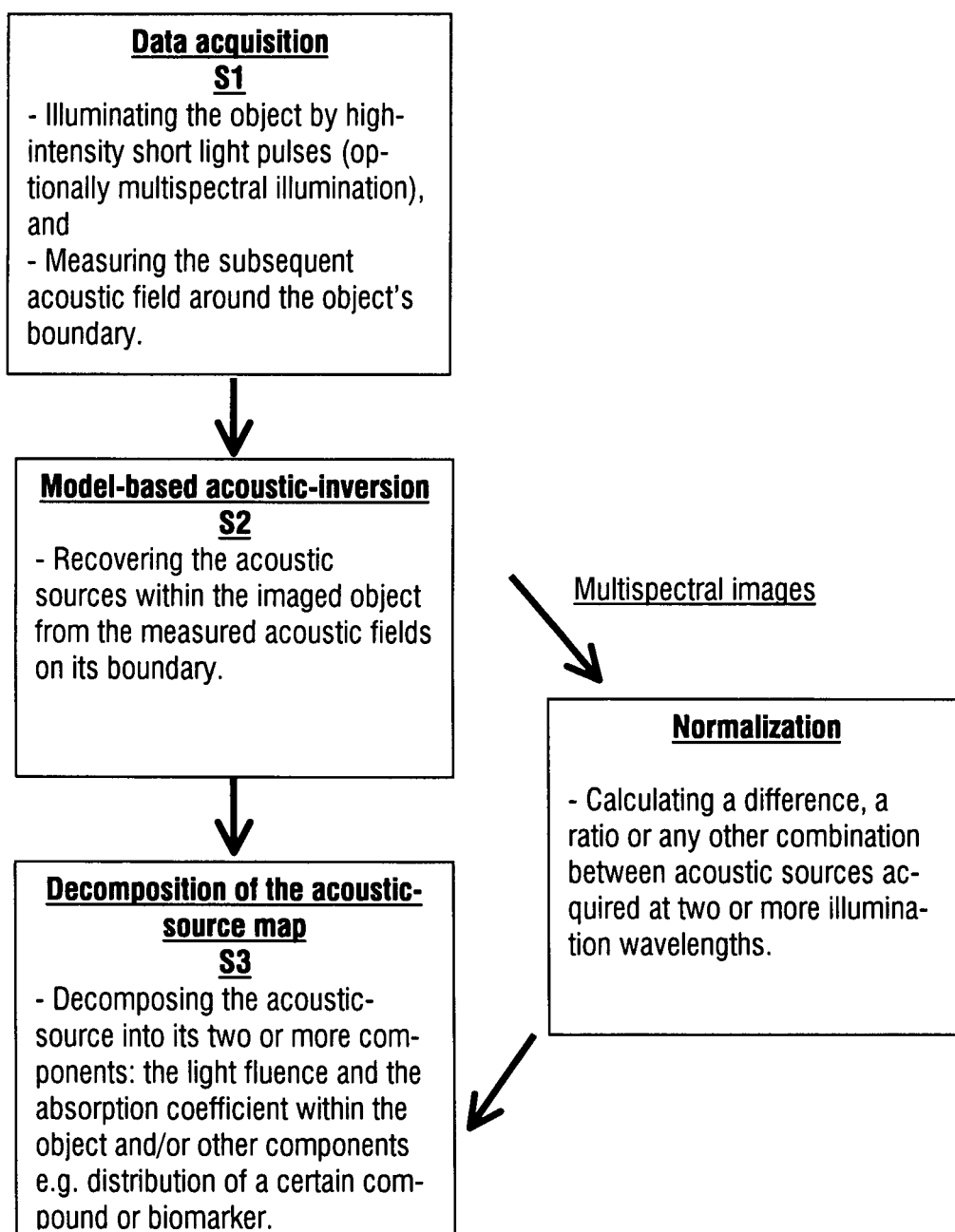


FIG. 1

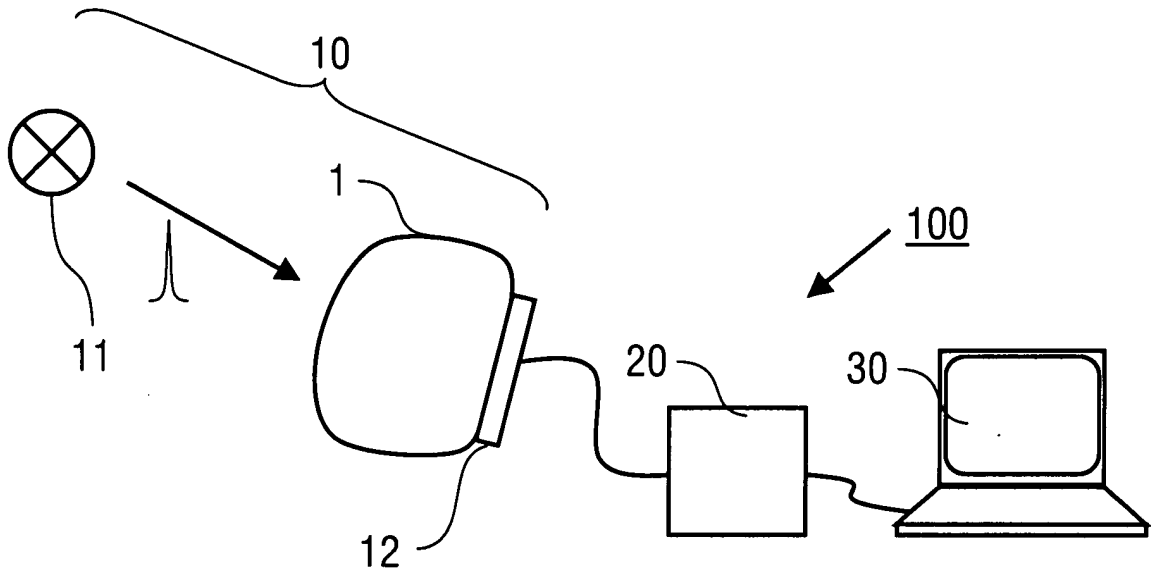


FIG. 2

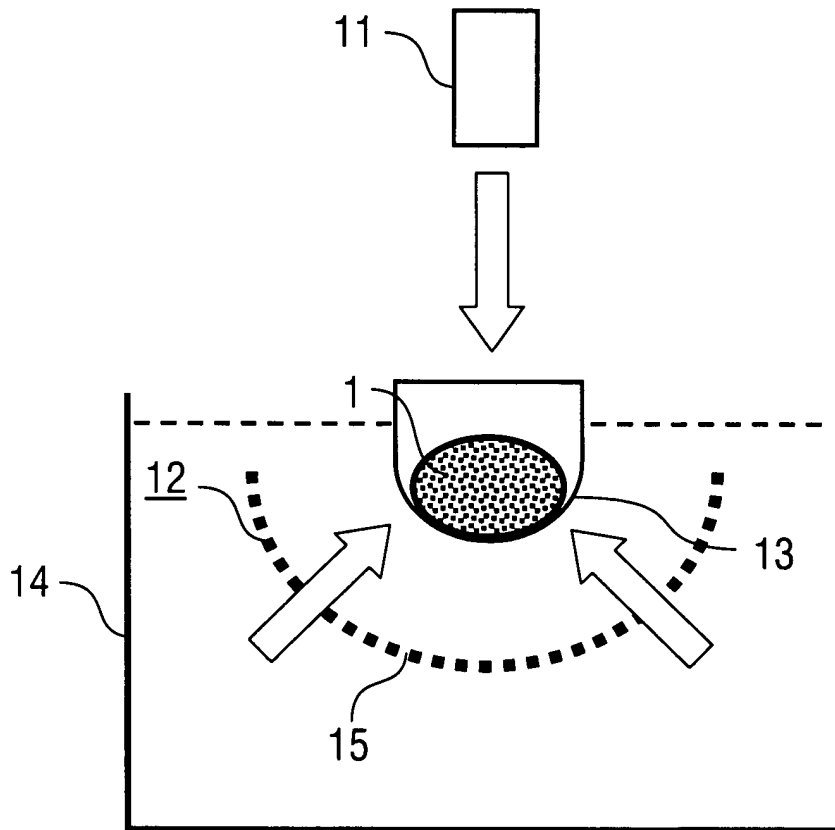


FIG. 3

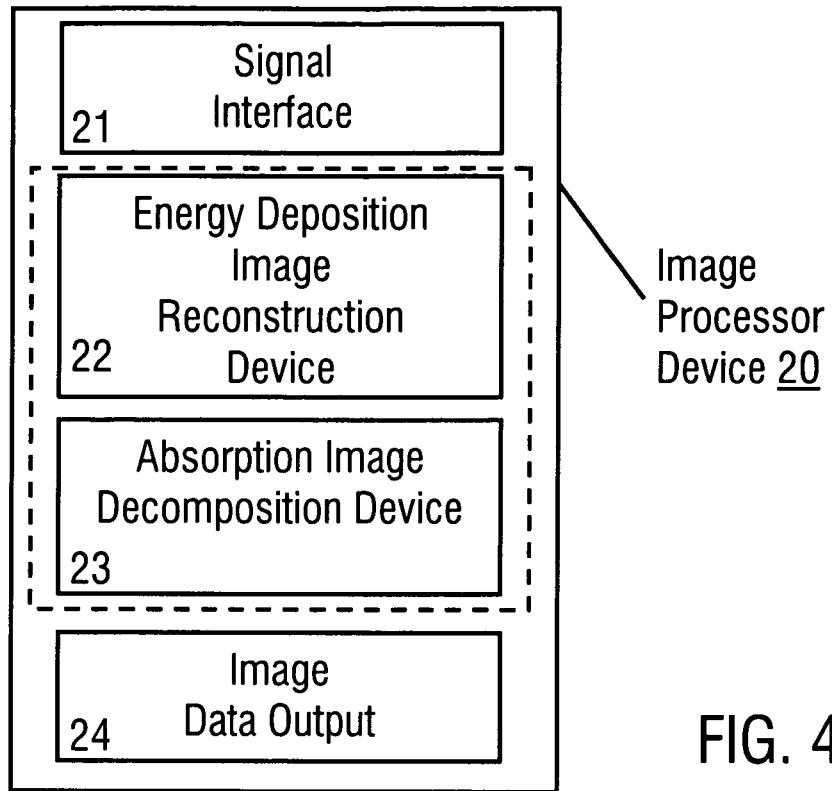


FIG. 4

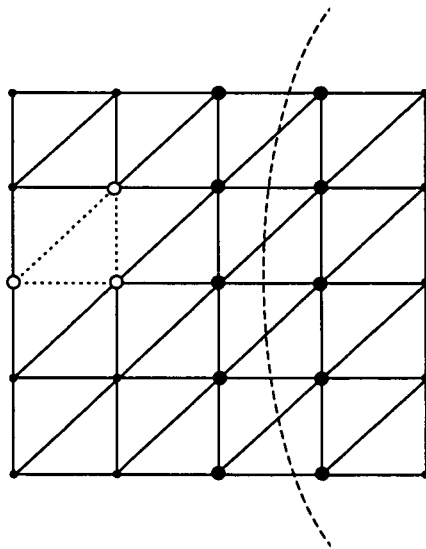


FIG. 5

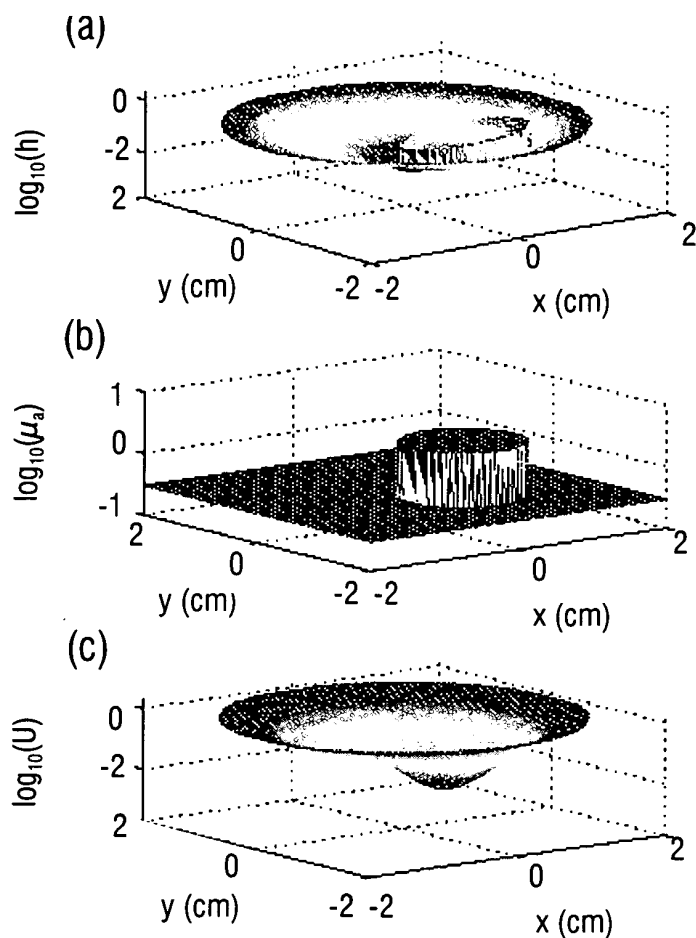


FIG. 6

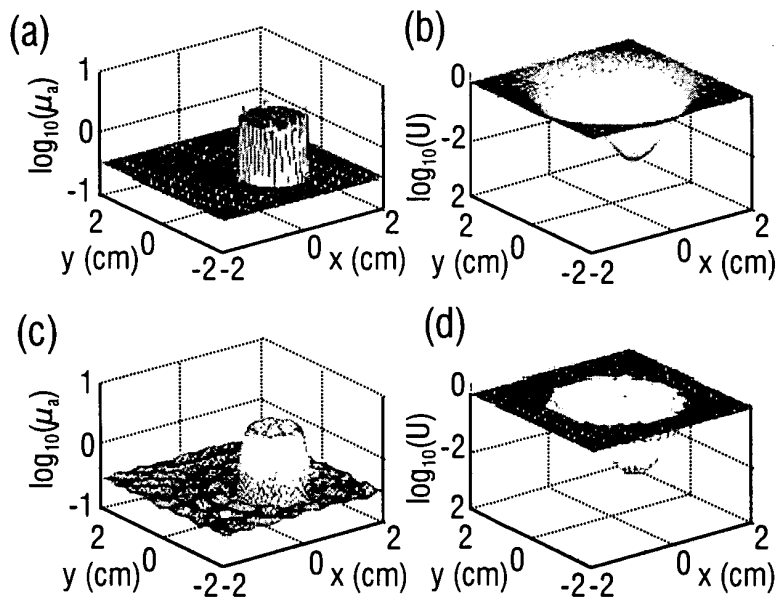


FIG. 7

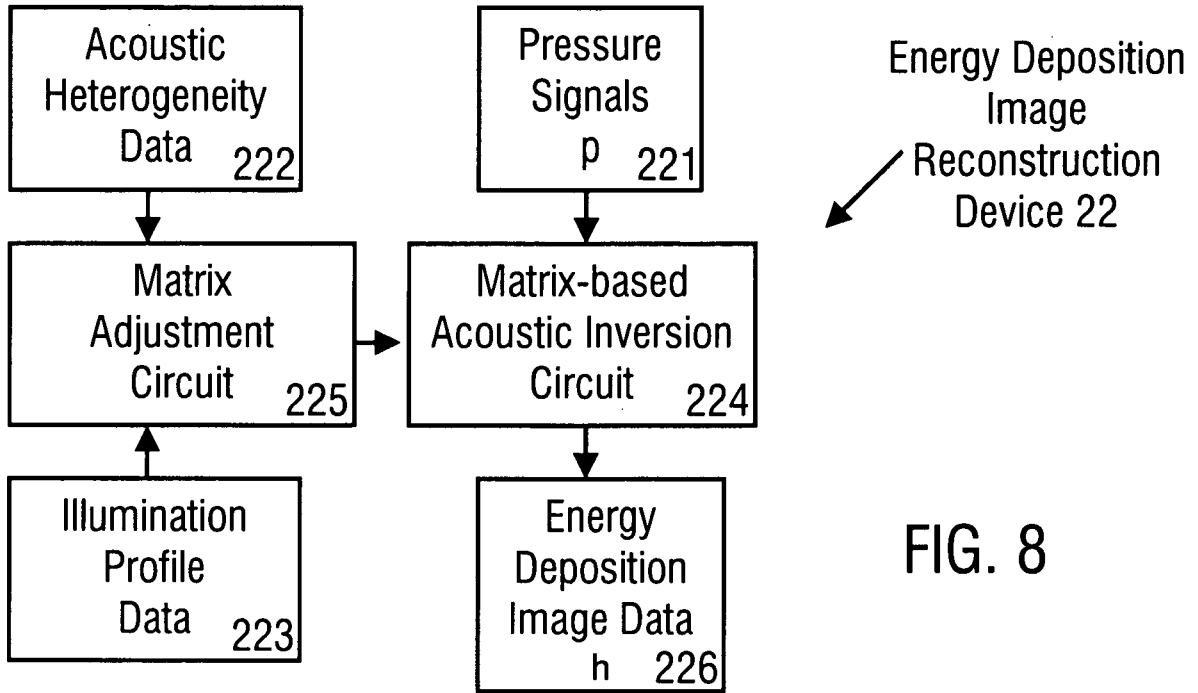


FIG. 8

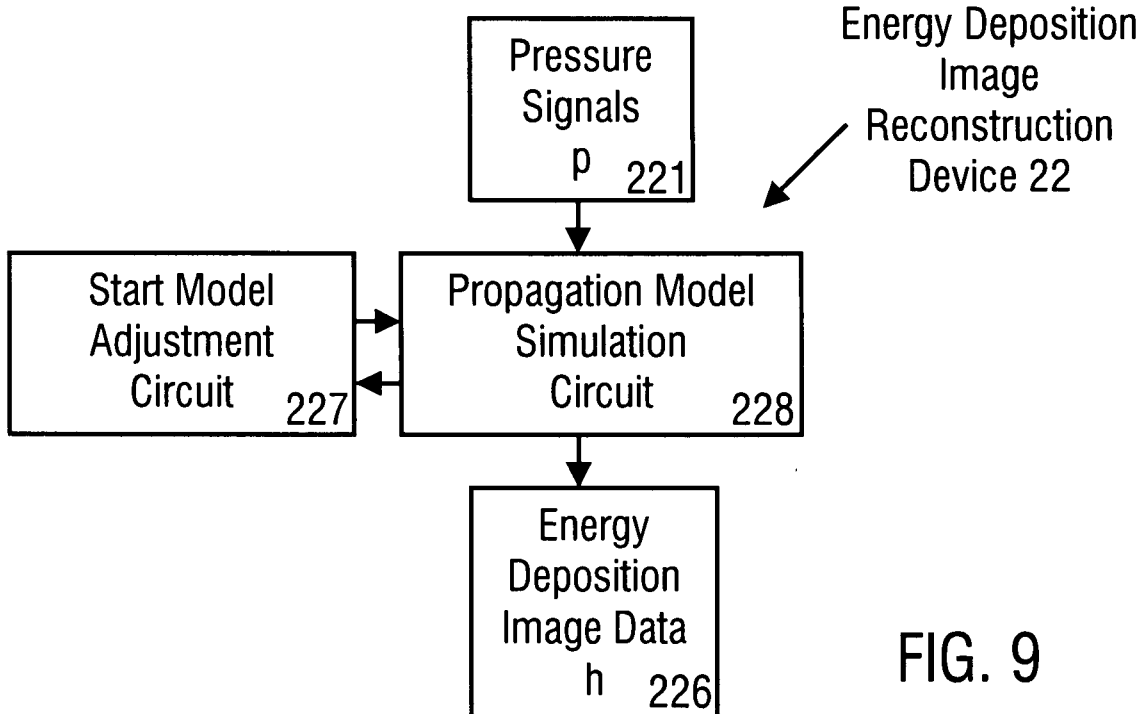


FIG. 9

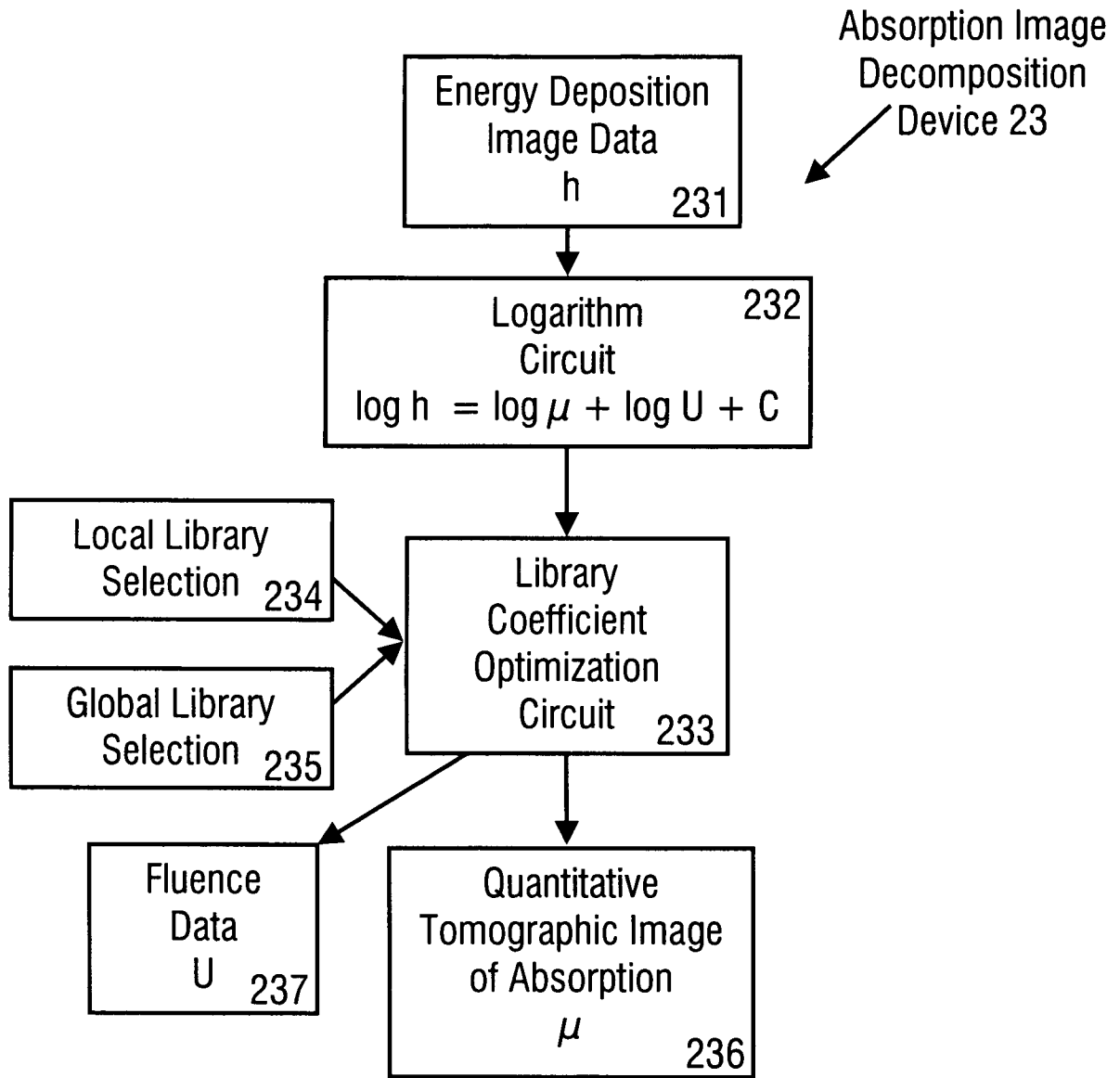


FIG. 10

**REFERENCES CITED IN THE DESCRIPTION**

*This list of references cited by the applicant is for the reader's convenience only. It does not form part of the European patent document. Even though great care has been taken in compiling the references, errors or omissions cannot be excluded and the EPO disclaims all liability in this regard.*

**Patent documents cited in the description**

- EP 2008006142 W [0008] [0037]

**Non-patent literature cited in the description**

- **H. JIANG et al.** *J. Opt. Soc. Am.*, 2006, vol. A (23), 878-888 [0006]
- **G. PALTAUF et al.** *The Journal of the Acoustical Society of America*, 2002, vol. 112 (4), 1536-44 [0006]
- **B. T. COX et al.** *Applied Optics*, 2006, vol. 45, 1866-1875 [0009]
- **B. T. COX BT et al.** *Proc SPIE*, 2007, vol. 6437 [0009]
- **JETZFELLNER et al.** *Appl. Phys. Lett.*, 2009, vol. 95 (1 [0009]
- **D. RAZANSKY ; V. NTZIACHRISTOS.** *Med.. Phys.*, 2007, vol. 34, 4293-4301 [0049]
- **S. S. CHEN et al.** *SIAM Review*, 2001, vol. 43, 129-159 [0077]

专利名称(译)	热声成像定量提取吸收图		
公开(公告)号	<a href="#">EP2449362B1</a>	公开(公告)日	2016-09-28
申请号	EP2009776877	申请日	2009-06-29
申请(专利权)人(译)	亥姆霍兹慕尼黑中心的德国研究中心的健康和环境 ( GMBH )		
当前申请(专利权)人(译)	亥姆霍兹慕尼黑中心的德国研究中心的健康和环境 ( GMBH )		
[标]发明人	RAZANSKY DANIEL NTZIACHRISTOS VASILIS ROSENTHAL AMIR		
发明人	RAZANSKY, DANIEL NTZIACHRISTOS, VASILIS ROSENTHAL, AMIR		
IPC分类号	G01N21/17 A61B5/00 A61B5/1455		
CPC分类号	A61B5/0095 A61B5/0059 A61B5/0093 G01N21/17 G01N21/1702		
其他公开文献	EP2449362A1		
外部链接	<a href="#">Espacenet</a>		

摘要(译)

一种物体的热声成像方法，包括以下步骤：提供表示对电磁能量输送到成像物体中的机械波响应的热声信号，基于热声信号重建表示物体内部能量吸收的能量沉积图像并且，将能量沉积图像分解为表示物体中的局部吸收系数和至少一个其他图像成分的分布的定量吸收图像。优选地，能量沉积图像重建步骤包括利用反演模型矩阵方法提供热声信号传播的前向模型矩阵和热声信号的基于矩阵的声学反演。此外，描述了一种成像装置，其适于进行物体的热声成像。

$$\begin{aligned}
 & \frac{\partial^2 p(\mathbf{r}, t)}{\partial t^2} - c^2 \nabla^2 p(\mathbf{r}, t) = \frac{\partial^2 q(\mathbf{r}, t)}{\partial t^2} \\
 & \frac{\partial^2 p(\mathbf{r}, t)}{\partial t^2} - c^2 \nabla^2 p(\mathbf{r}, t) = \frac{\partial^2 q(\mathbf{r}, t)}{\partial t^2} \\
 & \frac{\partial^2 p(\mathbf{r}, t)}{\partial t^2} - c^2 \nabla^2 p(\mathbf{r}, t) = \frac{\partial^2 q(\mathbf{r}, t)}{\partial t^2} \\
 & \frac{\partial^2 p(\mathbf{r}, t)}{\partial t^2} - c^2 \nabla^2 p(\mathbf{r}, t) = \frac{\partial^2 q(\mathbf{r}, t)}{\partial t^2}
 \end{aligned}$$